Nhlh1 and Nhlh2, a global transcriptional mechanism regulating commissural axon projection via activating Robo3

Aki Masuda, Rieko Ajima, Yumiko Saga, Tatsumi Hirata, Yan Zhu*

National Institute of Genetics, Graduate University for Advanced Studies, Sokendai, Yata 1111, Mishima, Shizuoka 411-8540, Japan

***Correspondence**: yanzhu@nig.ac.jp

Running Title: Nhlh1/2 control contralateral axon projection via Robo3

Key words: commissural neurons, contralateral projection, Robo3, bHLH, transcription factor, Nhh1, Nhlh2

SUMMARY

Commissural neurons play the crucial role to connect neuronal information from both sides of the nervous system in bilaterians by projecting their axons contralaterally across the midline. These neurons are highly heterogenous in their developmental origins, neurotransmitters and neurophysiology, as many disparate neuron classes contain commissural neurons. In mammals, most commissural axons from the spinal cord to the midbrain, cross the midline via the floor plate, guided predominantly by a conserved molecular mechanism, i.e., Robo3 and DCC expressing commissural axons are guided by Netrin-1 secreted from the floor plate and ventral neural tube. So far, no common transcriptional program has been uncovered for specifying the axon laterality across the highly heterogenous commissural neurons. In this study, we identified a pair of highly-related basic helix-loop-helix (bHLH) transcription factors, Nhlh1 and Nhlh2, as such a transcriptional program. We found that Robo3 promoter contains multiple copies of Nhlh1/2 binding sites and forced expression of Nhlh1/2 can induce ectopic Robo3 expression and contralateral axon projection in the hindbrain and the midbrain. We then generated mutant mice deficient in both genes and found a marked reduction of Robo3 and a total lack of ventral commissures from the spinal cord to the midbrain. This is the first report of a global transcriptional mechanism that controls the laterality of all floor plate-crossing commissural axons via activating Robo3 expression. Nhlh1 and Nhlh2 should provide the key to deciphering the principle underlying the specific and balanced production of contralateral- versus ipsilateral-projection neurons from the spinal cord to the midbrain.

INTRODUCTION

In bilaterians, neuronal information must be communicated between the two halves of the central nervous systems (CNS) for the normal functions of the animals, such as respiration, locomotion, visual and auditory processing (Borst and Soria van Hoeve, 2012; Bouvier et al., 2010; Goulding, 2009; Kiehn, 2016; Lanuza et al., 2004; Petros et al., 2008). This crucial task is achieved by commissural neurons that project their axons across the midline of the neural tube to connect with their target neurons on the contralateral side. Evolution of commissural circuits organization might underlie the emergence of new functions, such as quadrupedal locomotion and binocular vision (Friocourt et al., 2019; Kiehn, 2016; Petros et al., 2008).

Many diverse neuron classes, defined developmentally by distinct combinations of transcription factors (TFs), contain commissural neurons, and often each neuron class contains a mixture of commissural and ipsilaterally-projecting neurons (Alaynick et al., 2011; Lai et al., 2016; Tulloch et al., 2019). Therefore, commissural neurons are highly heterogenous in terms of their developmental origin, morphology, neurotransmitter type, connectivity, and neurophysiology (Chédotal, 2014; Tulloch et al., 2019), but all share the core defining feature of projecting their axons across the midline. Despite their heterogeneity, the axon guidance mechanisms that direct commissural axons to reach and cross the midline, are fairly conserved and well understood (Chédotal, 2011, 2019; Comer et al., 2019). By contrast, the transcriptional programs that specify the laterality of commissural axons, and furthermore, whether a global regulatory mechanism operates for diverse commissural neurons, are little understood.

In vertebrates, most commissural neurons in the spinal cord, hindbrain and midbrain project ventrally to cross the midline at the floor plate (FP) (Friocourt et al., 2019). The FP does not extend beyond the midbrain, therefore is missing in the forebrain (Placzek and Briscoe, 2005). Guidance of commissural axons towards the FP predominantly relies on the interaction between the ligand Netrin-1, which is expressed from the FP and the ventral neural progenitors, and two receptor molecules Robo3 and DCC expressed in the commissural neurons (Dominici et al., 2017; Fazeli et al., 1997; Kennedy et al., 1994; Marillat et al., 2004; Moreno-Bravo et al., 2019; Sabatier et al., 2004; Serafini et al., 1996; Tamada et al., 2008; Varadarajan et al., 2017; Yamauchi et al., 2017). Another ligand receptor pair, Shh and Boc, makes an additional but minor contribution to this process (Charron et al., 2003; Okada et al., 2006; Wu et al., 2019). Knockout (KO) mice of Netrin-1, or DCC or Robo3 all showed disrupted ventral commissure formation, among which Robo3 KO showed a complete lack of ventral commissure in the spinal cord and the hindbrain (Fazeli et al., 1997; Laumonnerie et al., 2015; Marillat et al., 2004; Sabatier et al., 2004; Serafini et al., 1996; Tamada et al., 2008). While DCC directly interacts with Netrin-1, Robo3 cannot (Zelina et al., 2014). The mammalian Robo3 binds DCC and facilitates Netrin-1 downstream signaling, thereby promoting commissural axons to extend towards the midline (Zelina et al., 2014). Robo3 is transiently expressed in pre-crossing but becomes quickly downregulated in post-crossing commissural axons/neurons (Marillat et al., 2004; Sabatier et al., 2004). Up to date, Robo3 is the only known molecule that is exclusively expressed in the commissural neurons from the spinal cord to the midbrain (Friocourt et al., 2019; Inamata and Shirasaki, 2014; Marillat et al., 2004; Sabatier et al., 2004; Tamada et al., 2008; Tulloch et al., 2019). DCC, however, is also expressed in

some ipsilaterally-projecting neurons (Bai et al., 2011; Dillon et al., 2005; Keino-Masu et al., 1996). Therefore, how Robo3 expression is transcriptionally regulated is likely to be the core of the transcriptional program that specifies commissural identity.

There is very limited knowledge on how Robo3 transcription is regulated in commissural neurons. LIM-homeodomain TFs, Lhx2/9, have been shown to control Robo3 expression in the commissural neurons of dI1 spinal neurons, and Lhx2 is able to bind to Robo3 promoter (Wilson et al., 2008). However, there is no evidence to suggest that Lhx2/9 can account for Robo3 expression beyond dI1 spinal neurons. In the midbrain and the preBötzinger complex in the hindbrain, neural progenitors expressing homeobox gene Dbx1 give rise to commissural neurons (Bouvier et al., 2010; Inamata and Shirasaki, 2014). Knockout or knockdown of Dbx1 affected contralateral axon projections, whilst forced expression of Dbx1 in the midbrain induced ectopic Robo3 expression and contralateral axon projection. However, Dbx1 also is an unlikely solution to account for Robo3 expression beyond those commissural neurons derived from the Dbx1-positive progenitor domains. Moreover, Dbx1, whose expression is confined to neural progenitors, cannot directly regulate the expression of Robo3 which is expressed in the post-mitotic young neurons. Therefore, up to date, we still do not know whether Robo3 is separately regulated by different sets of TFs in distinct classes of commissural neurons, or there exists a common transcriptional mechanism for all FP-crossing commissural neurons. The fact that a highly conserved Robo3 spatial and temporal distribution has been observed across divergent vertebrate species might indicate that common upstream regulators are likely to operate (Friocourt et al., 2019).

In this study, we attempted to uncover transcriptional mechanisms that specify axon laterality in commissural neurons. We reasoned that components of an immediate upstream regulatory program are likely to be enriched in the pre-crossing versus post-crossing commissural neurons, reflecting the temporal dynamics of Robo3 (Marillat et al., 2004; Sabatier et al., 2004). Based on this assumption, we took advantage of the result from our RNA-seq experiment which compared transcriptomes between pre-crossing and post-crossing pontine nucleus (PN) neurons in the murine hindbrains, and identified an enrichment of a pair of closely-related basic helix-loop-helix (bHLH) TFs, Nhlh1 and Nhlh2, in the pre-crossing population. Nhlh1 and Nhlh2 (previously also named: Nscl1/2, Hen1/2) are expressed in immature neurons (Duncan et al., 1997; Haire and Chiaramello, 1996; Murdoch et al., 1999; Theodorakis et al., 2002), but their roles in neural development have not been thoroughly explored, particularly in the context of double deficiency of both genes (Krüger and Braun, 2002; Krüger et al., 2004; Schmid et al., 2007). We found that the Robo3 promoter contains multiple copies of Nhlh1 and Nhlh2 binding sites, and that forced expression of Nhlh1 and Nhlh2 could induce ectopic Robo3 expression. By generating loss of function Nhlh1 and Nhlh2 mouse lines, we were able to show that deficiency in both Nhlh1 and Nhlh2 leads to a marked reduction of Robo3 transcription, and a total disruption of FP-crossing commissures, from the spinal cord to the midbrain.

RESULTS

To separate pure pre-crossing and post-crossing commissural neurons are not trivial, as during development the pre-crossing and the post-crossing, as well as the commissural and the ipsilateral-projecting neurons, intermingle spatially. We,

therefore, turned to a specialized group of commissural neurons, the precerebellar PN neurons in the hindbrain, whose cell bodies migrate tangentially over a considerable distance from the dorsal edge of the hindbrain to settle next to the ventral midline (Kawauchi et al., 2006; Okada et al., 2007; Shinohara et al., 2013). The migration of PN neurons is steered and pulled anteroventrally by their leading processes towards the midline, which requires Netrin-1/ DCC/Robo3 signaling (Marillat et al., 2004; Yee et al., 1999). While the leading processes cross the midline, the cell bodies of most PN neurons terminate their migration without midline crossing. This developmental feature enables considerable spatial separation of two PN populations: those in the early- and mid-migratory route harboring the pre-crossing, and those near the midline region harboring the post-crossing leading processes. We took advantage of this feature to obtain pure populations of pre- and post-crossing PN neurons and compared their transcriptomic profiles (results to be published elsewhere). We found that a pair of highly related class II bHLH TFs, Nhlh1 and Nhlh2, were highly enriched in the pre-crossing (during migration), but became markedly down-regulated in the post-crossing (at destination), PN neurons (enrichment fold: 54.52 for Nhlh1, 9.88 for Nhlh2). This differential expression of Nhlh1 and Nhlh2 was confirmed by the in situ hybridization (ISH) expression data from the Allen Developing Mouse Brain Atlas (https://developingmouse.brain-map.org/) (Supplemental Fig. 1).

Nhlh1 and Nhlh2 could induce Robo3 expression as transcription activators

The enrichment of Nhlh1 and Nhlh2 in pre-crossing PN neurons suggests that they might regulate the expression of genes required for the behaviors of the pre-crossing PN neurons. We therefore screened for Nhlh1/2 binding sites in the promoters of the

transcripts that are enriched in pre-crossing PN population from our RNA-seq data using the position frequency matrices (PFMs) of Nhlh1 and Nhlh2 from JASPAR. The screen found that the promoter of Robo3, a gene known to be highly expressed in migrating PN neurons (Marillat et al., 2004), bears multiple copies of potential Nhlh1/2 binding sites. Using the FIMO tool of the MEME Suite and the Eukaryotic Promoter Databases, we scanned the proximal 2 kb promoter sequences of Robo3, and found seven statistically significant matches to the consensus Nhlh1/2 binding sequences (Fig. 1A). We next aligned the promoter sequences of Robo3 from five divergent mammalian species and identified a highly conserved region. Presence of the so-called phylogenetic footprints, though not a direct proof, implies the potential importance of the conserved regions for the regulation of Robo3 transcription. We found a highly conserved region within the 150 bp region proximal to the transcriptional start site (TSS) (Fig. 1B), which contains a Nhlh1/2 binding site of high matching probability (Fig. 1A, C). The results from the in silico analysis raised the possibility that Nhlh1 and Nhlh2 might regulate Robo3 transcription.

We, therefore, tested if forced expression of Nhlh1 and Nhlh2 could induce ectopic Robo3 expression. We introduced expression vectors of full-length Nhlh1 and Nhlh2 into the lower rhombic lip of the E12.5 mouse hindbrains via in utero electroporation (EP) and analyzed Robo3 protein expression at E14.5 (Fig. 2A). The lower rhombic lip region situated at the dorsal edge of the caudal hindbrain (Fig. 2B) is the progenitor zone of the PN neurons (Altman and Bayer, 1987; Pierce, 1966; Rodriguez and Dymecki, 2000; Wingate and Hatten, 1999), but is devoid of Robo3 expression (Fig. 2C non-EP side, 2E) because the post-mitotic PN neurons only begin to express Robo3 after leaving the rhombic lip. Forced expression of Nhlh1 and Nhlh2 in the rhombic lip

clearly induced ectopic expression of Robo3 within the rhombic lip region (Fig. 2C, C', C'', D, D', D''). Electroporated neurons found deep within the hindbrain neuroepithelium also expressed ectopic Robo3 (Fig. 2F, F', F''). Ectopic Robo3 induction was also observed when Nhlh1 and Nhlh2 were electroporated into the midbrain (Fig. 2G, H, H', I, I', I'' compared to J). EP of Nhlh1 or Nhlh2 alone also induced ectopic Robo3 expression in the rhombic lip and the midbrain, though appeared to be less efficient than Nhlh1 and Nhlh2 combined (Supplemental Fig. 2). On the contrary, EP of full-length Lhx2, a molecule previously shown to directly control Robo3 transcription in the dI1 spinal neurons (Kawauchi et al., 2010; Wilson et al., 2008), did not induce ectopic Robo3 expression in the rhombic lip and the midbrain (Supplemental Fig. 3). Robo3 ISH was next performed on EP samples and indicated that the ectopic expression of Robo3 is induced at the transcription level (Supplemental Fig. 4). These results, taken together, suggest that Nhlh1 and Nhlh2 regulate Robo3 transcription.

Next, we asked whether Nhlh1 and Nhlh2 function as transcriptional activator or repressor, and furthermore, what domains of these molecules are important for induction of Robo3. Nhlh1 and Nhlh2 share a highly homologous canonical bHLH domain in the C-terminus half and a poorly conserved low complexity domain in the N-terminus half (Fig 3A) (Begley et al., 1992; Brown et al., 1992). In between the two domains, both molecules contain a highly conserved stretch of 11 amino acids, encompassing six or five consecutive arginine, immediately preceding the canonical bHLH domain. This stretch, which we named as R6 domain, is a feature specific to Nhlh1 and Nhlh2 (Begley et al., 1992; Brown et al., 1992). The highly charged R6 domain may form an extended basic domain together with the canonical basic region,

rendering DNA binding specificity unique to Nhlh1/2 (Brown and Baer, 1994). Evidence exists on both sides for a role of Nhlh1/2 as an activator or a repressor (Good and Braun, 2013; Isogai et al., 2011; Krüger et al., 2004; Manetopoulos et al., 2003; Wankhade and Good, 2011). If Nhlh1/2 induce Robo3 expression by directly binding to its promoter, a possibility suggested by our in silico analysis, it would imply that Nhlh1/2 should work as transcriptional activators. To test this possibility, we generated two types of Nhlh1/2 fusion molecules: (1) fusion with a potent trans-activating domain from the herpes simplex virus TF VP16 (Sadowski et al., 1988); (2) fusion with a potent repressor domain, EnR, from the drosophila Engrailed (Fan and Sokol, 1997) (Fig. 3B). We electroporated the fusion constructs into the E12.5 brainstems as in Figure 2 and assayed for Robo3 induction in the rhombic lip and the midbrain. The VP16-fused full length Nhlh1/2 strongly induced Robo3 expression in the rhombic lip (Fig. 3E) as well as in the midbrain (Supplemental Fig. 5A). By contrast, EnR-fused Nhlh1/2 failed to induce ectopic Robo3 expression in the rhombic lip (Fig. 3F) and in the midbrain (Supplemental Fig. 5B). These results suggest that indeed Nhlh1/2 serve as transcriptional activators in inducing Robo3 expression. We next asked the functional importance of R6 domain in Robo3 induction. We found that VP16 fused canonical bHLH domain without the R6 domain did not induce Robo3 expression (Fig. 3G, Supplemental Fig. 5C), whereas VP16 fused R6-containing bHLH domain was a potent inducer of Robo3 (Fig. 3H, Supplemental Fig. 5D). This result suggests that the R6 domain unique to the Nhlh1/2 subfamily, together with the canonical bHLH domain, are essential for Nhlh1/2 to activate the expression of Robo3.

Forced expression of Nhlh1/2 drives contralateral axon projections

So far, we showed that forced Nnhlh1 and Nhlh2 expression induced ectopic Robo3 expression. But can it instruct axon projection towards the ventral midline? To answer this question, we force-expressed Nhlh1 and Nhlh2 in the developing hindbrain and midbrain as in Figure 2, and examined the axon trajectories of the electroporated neurons. In the midbrain, we employed a previously established method that enabled examination of axon laterality on flat-mounted brainstem after in utero EP (Fig. 4A) (Inamata and Shirasaki, 2014). EP with an mCherry expression construct into the midbrain at E11.5 labelled chiefly caudally-extending ipsilateral axons, in line with the previous report (Fig. 4B, 4C) (Inamata and Shirasaki, 2014). Forced expression of Nhlh1 and Nhlh2 with mCherry at E11.5, on the other hand, could direct some of these neurons to project contralaterally (Fig. 4B, 4C). In the hindbrain, control EP with a GFP construct at E12.5 labelled only few neurons whose axons extend ventrally towards midline, resulting in low levels of GFP fluorescence near the midline region (Fig. 4D, E). EP of Nhlh1 and Nhlh2 with GFP, by contrast, labelled numerous neurons that either extended their axons or migrated themselves towards the midline (Fig. 4D, E). The GFP signal near the midline was significantly higher than that of the control (Fig. 4E). These results from both the hindbrain and the midbrain show that forced expression of Nhlh1/2 could certainly drive changes in axonal projection from ipsilateral to contralateral, suggesting that axon laterality in vivo could be determined by the presence or absence of a pair of TFs.

Expression of Nhlh1, Nhlh2 in relation to Robo3 during the development of commissural neurons

Co-localization of Nhlh1 and Nhlh2 with Robo3 should be a strong indicator of whether and where in the CNS these molecules may regulate Robo3 transcription. Robo3 has been previously shown to be expressed and required in almost all commissural neurons whose axons cross the ventral midline at the FP, which spans from the spinal cord to the midbrain (Friocourt et al., 2019; Inamata and Shirasaki, 2014; Marillat et al., 2004; Sabatier et al., 2004; Tamada et al., 2008). The FP ceases to exist rostral to the midbrain (Placzek and Briscoe, 2005), hence Robo3 expression in the forebrain might be involved in other functions. We examined the expression patterns of Nhlh1 and Nhlh2 in relation to that of Robo3 in areas and at stages where and when FP-crossing commissural axon projections take place.

Because good antibodies to detect or distinguish Nhlh1 and Nhlh2 are unavailable, we turned to ISH using Nhlh1, Nhlh2, and Robo3 riboprobes on adjacent sections. Nhlh1, Nhlh2 and Robo3 expression were first examined in the migrating PN neurons at E14.5. In agreement with our RNA-seq data and the ISH expression data from the Allen Developing Mouse Brain Atlas (https://developingmouse.brain-map.org/) (Supplemental Fig. 1), we found that both Nhlh1 and Nhlh2 are expressed in migrating PN neurons similarly to Robo3 expression (Fig. 5A). Next, we examined the expression of these three molecules across the entire neuroaxis of the CNS at E11.5 and E13.5, stages when most commissural neurons project axons towards the ventral midline. We found that Robo3 generally labelled neurons immediately adjacent to the ventricular zone, a region where young immature neurons reside, but not the more differentiated neurons in superficial positions (Fig. 5B, C, D, E, F, G, H). This is consistent with the previous findings that Robo3 is transiently expressed in pre-crossing commissural neurons, and becomes downregulated soon after commissural axons cross

the midline (Marillat et al., 2004; Sabatier et al., 2004). Remarkably, from the spinal cord to the midbrain, Nhlh1 and Nhlh2 are expressed in areas which also express Robo3 (Fig. 5B, C, D, E, F, G, H). Two points should be noted. First, Nhlh1 and Nhlh2 expression combined together appears wider than that of Robo3, which is more obvious at E11.5 than E13.5. For example, Nhlh1 and Nhlh2 seem to be expressed, albeit weakly, in the ventral spinal cord which is largely devoid of Robo3 (Fig. 5B). Likewise, in the E11.5 caudal and rostral hindbrains (Fig. 5D, F), Nhlh2 in particular showed expression in more differentiated neurons located superficially. Second, the relative strength of Nhlh1 and Nhlh2 expression appear to vary depending on brain regions and neuronal subdomains. For example, Nhlh1 expression appears to be stronger than Nhlh2 in the ventral-most spinal domain, whereas Nhlh2 appears stronger for the dorsal spinal cord (Fig. 5B). Despite the varying relative strength of expression, Nhlh1 and Nhlh2 expression domains are mostly overlapping. In the E11.5 midbrain, Nhlh1 signal is very weak, but is still present as a faint band of signal correlating to Robo3 pattern. These results from the expression study of Nhlh1, Nhlh2 and Robo3 suggest: (i) a high likelihood that Nhlh1 and Nhlh2 may regulate Robo3 expression in vivo in most commissural axons that cross midline via the FP; (ii) Nhlh1 and Nhlh2 may functionally complement each other. In brain regions rostral to the midbrain, however, Robo3 and Nhlh1 and Nhlh2 expression became much less correlated (Supplemental Fig. 6).

FP-crossing commissural axons from the spinal cord to the midbrain fail to approach the ventral midline in Nhlh1 and Nhlh2 double deficient mice

To examine the endogenous function of Nhlh11 and Nhlh2, we generated Nhlh1 and Nhlh2 deficient mice by CRISPR/Cas9 mediated gene editing in germ line cells (Supplemental Fig. 7A, B). The resultant Nhlh1 mutant allele (Nhlh1-m) carries a premature termination site just before the first helix region, hence generating a truncated Nhlh1 protein without the HLH region (Supplemental Fig. 7C). The Nhlh2-m allele carries corrupted amino acids over the extended basic domain and the first helix regions (Supplemental Fig. 7D), resulting in a peptide which could no longer generate the bHLH structure. Given that the bHLH region is essential for DNA binding and protein-protein interaction for bHLH TFs (Bertrand et al., 2002; Dennis et al., 2019), we expected that the Nhlh1-m and Nhlh2-m were likely to be loss-of-function alleles. To confirm this, we cloned the coding sequences of Nhlh1-m and Nhlh2-m into an expression vector. Forced expression of Nhlh1-m and Nhlh2-m into E12.5 mouse embryos by EP as in Figure 2 did not induce ectopic expression of Robo3 in the rhombic lip (Supplemental Fig. 7E). We also confirmed that Nhlh1-m and Nhlh2-m expression did not act dominant negatively in suppressing Robo3 expression, as PN neurons expressing Nhlh1-m and Nhlh2-m showed normal Robo3 expression (Supplemental Fig. 7F).

We then went on to generate mice that were single and double homozygotes of Nhlh1-m and Nhlh2-m. Targeted knockout of Nhlh1 and Nhlh2 have been previously generated (Cogliati et al., 2002; Good et al., 1997; Krüger and Braun, 2002) and so far besides perinatal lethality, only two defects in developing brain have been reported in the double knockout (dKO) mice: defects in the migration of PN neurons (Schmid et al., 2007), and the Gonadotropin releasing hormone expressing neurons (GnRH) (Krüger et al., 2004). However, the mechanisms underlying these defects have not been

illuminated. We first analyzed the PN formation in our mice. In the double Nhlh1/2 mutant, we found that PN neurons failed to migrate towards the ventral midline, but instead arrested migration in lateral and anteriorly-extended positions (Fig. 6A, B). This phenotype observed in our mice resembles what has been previously reported in the dKO mice (Schmid et al., 2007). PN formation in single Nhlh1 and Nhlh2 mutant appeared normal, again in line with what was reported previously (Supplemental Fig. 8) (Schmid et al., 2007). Interestingly, the PN phenotype observed in the present study and in the dKO before is highly reminiscent of the PN defect in the Robo3 mutant (Marillat et al., 2004). Another precerebellar nucleus, the inferior olivary nucleus (ION), was also affected in the Robo3 mutant (Di Meglio et al., 2008; Marillat et al., 2004). We therefore examined ION in our Nhlh1/2 double mutant. We found that in the double mutant, ION neurons failed to gather tightly around the ventral midline as in the control, but rather were situated at a small distance away from the midline, a phenotype again resembling that of the Robo3 mutant (Supplemental Fig. 9) (Di Meglio et al., 2008).

The correlated expression of Nhlh1, Nhlh2 and Robo3 in commissural neurons from the spinal cord to the midbrain prompted us to examine the ventral commissure formation throughout these regions in our mutant mice. Tag1 (also known as Contactin2) was used as a marker for commissural axons (Dodd et al., 1988; Yamamoto et al., 1986), and neurofilament (NF) for revealing the overall axonal patterns. We found that ventral commissures completely failed to form in the double mutant in the spinal cord (Fig. 7A,), caudal hindbrain (Fig. 7B), rostral hindbrain (Fig. 7C) and midbrain (Fig. 7D). The overall axonal patterns except the lack of ventral commissures, as well as the cytoarchitecture of these CNS regions shown by DAPI

staining, appeared grossly normal (Fig. 7). Tag1 positive axons initially developed normally but failed to converge and extend all the way to the ventral midline, which could be better appreciated on the spinal cord samples (Fig. 7A). No notable abnormality in the ventral commissure formation has been observed in the single mutants of Nhlh1 and Nhlh2 (Supplemental Fig. 10). The prevalent absence of ventral commissures persisted into later stages, as shown by analyses in E13.5 and E16.5 spinal cord (Supplemental Fig. 11A, B), and E13.5 hindbrain and midbrain (Supplemental Fig. 11C, D).

What about the non-FP crossing commissural axons, such as dorsally crossing commissural axons or commissures formed anterior to the midbrain where the FP ceases to exist, whose extension to the midline have been shown previously to be independent of Robo3 (Chédotal, 2014; Comer et al., 2015; Friocourt et al., 2019)? We asked whether these other types of commissural axons could form normally in our Nhlh1/2 double mutant. We found that the dorsal commissure in the spinal cord, the anterior commissure in the basal forebrain and the corpus callosum were all normally formed in the double mutant (Supplemental Fig. 12). This result indicates that Nhlh1/2 deficiency specifically affect commissural axons that cross the midline via the FP.

Marked reduction of Robo3 in Nhlh1 and Nhlh2 double mutant from the spinal cord to the midbrain

We showed that FP-crossing commissures failed to form in the Nhlh1/2 double mutant resembling the defect observed in the Robo3 mutant. We therefore investigated Robo3 expression in Nhlh1/2 double mutant by Robo3 Immunohistochemistry (IHC). We found a huge reduction of Robo3 expression in the E11.5 spinal cord (Fig. 8A),

caudal hindbrain (Fig. 8B), rostral hindbrain (Fig. 8C), and midbrain (Fig. 8D) in the double mutant compared to the control. Similarly, a marked reduction of Robo3 was also observed in the migrating PN neurons at E16.5 (Fig. 8E). Examining Robo3 transcription by ISH also found a huge reduction of Robo3 mRNA in the spinal cord (Fig. 8F), and the migrating PN neurons (Fig. 8G) in the double mutant. These results provide the ultimate proof that Nhlh1 and Nhlh2 transactivate Robo3 expression in vivo.

We believe that Robo3 deficiency is the main cause for the commissure-less phenotype for the following reasons. First, Robo3 was barely detectable in the Nhlh1/2 double mutant. Second, we examined the expression of Netrin-1 and Shh, the two main guidance molecules previously shown to guide commissural axons towards the midline (Charron et al., 2003; Kennedy et al., 1994; Serafini et al., 1996), and found that they were expressed in a comparable manner between the double mutant and the control (Supplemental Fig. 13). Third, the neurogenesis and initial axon extension of commissural neurons did not appear to be affected in the double mutants. This is because Tag1 and DCC, both predominantly expressed in commissural neurons, showed almost normal expression profile in the dorsal half of the spinal cord in the double mutant where most commissural neurons reside (Fig. 7A, Supplemental Fig. 14A). In addition, Brn3a+ neurons, which are dI1, dI2, dI3, dI5, and dILB spinal neuronal classes comprising a mixture of ipsilateral- and contralateral- projecting neurons (Lai et al., 2016; Tulloch et al., 2019), were comparable in numbers between the double mutant and the control (Supplemental Fig. 14B). Similarly, the specification of the PN neurons also appeared to be normal in the double mutant as these neurons migrated

anteriorly and expressed PN neuronal marker Barhl1 and DCC (Fig. 6, Supplemental Fig. 14C).

Robo3 expression rostral to the midbrain is not affected in Nhlh1/2 double mutant

The seemingly uncorrelated expression of Nhlh1, Nhlh2 and Robo3 in structures rostral to the midbrain (Supplemental Fig. 6) raised the possibility that Robo3 expression in these structures might not be affected in the Nhlh1/2 double mutant. To test this prediction, we examined Robo3 expression in three forebrain structures known to express Robo3: the ganglionic eminence (GE), the medial habenular nucleus (mHb) and the hypothalamus (HTH) (Supplemental Fig. 6) (Barber et al., 2009; Belle et al., 2014; Quina et al., 2009; Schmidt et al., 2014). We found no differences in Robo3 expression levels in the GE, the mHb and the HTH between the double mutant and the control (Supplemental Fig. 15A, B, C). Axons from the mHb form a highly fasciculated Fasciculus Retroflexus (FR), which projects caudally through the midbrain and turn to cross the ventral midline at the midbrain/hindbrain junction (Belle et al., 2014). We found that the FR in the double mutant continued to express Robo3 (Supplemental Fig. 15D) and was able to approach and cross the ventral midline (Supplemental Fig. 15E), which supported our earlier conclusion that the extrinsic guidance program for midline crossing is intact in the double mutant. These results, taken together, suggest that Robo3 expression in the forebrain is controlled by transcriptional program other than Nhlh1/2.

DISCUSSION

In this study, we have uncovered a transcriptional program, involving bHLH TFs, Nhlh1 and Nhlh2, for regulating the contralateral projection of commissural axons in mice. We initially identified these molecules in a specialized commissural system, the hindbrain PN neurons. Remarkably, mice deficient of both molecules reveal that Nhlh1 and Nhlh2 have a global function in all FP-crossing commissural neurons from the spinal cord to the midbrain. We have further shown that Nhlh1 and Nhlh2 regulate laterality of commissural axons by transactivating Robo3 expression. To our knowledge, this is the first study to show that a common gene regulatory program operates upstream of Robo3 to regulate commissural axon projection. Our study has brought to the fore a pair of relatively under-explored bHLH molecules, which should serve as a key to decipher the mechanisms that control the precise and balanced production of commissural neurons.

Nhlh1 and Nhlh2, as transcriptional activators of Robo3 expression

We show that Nhlh1 and Nhlh2 function as transcriptional activators in Robo3 induction and that the R6 domain is crucial for their function. Nhlh1/2 belong to the TAL1/SCL subfamily of class II bHLH TFs (Begley et al., 1992; Brown et al., 1992). As with all bHLH TFs, the HLH domain mediates protein interactions, and the basic domain directs DNA binding (Bertrand et al., 2002; Dennis et al., 2019). Nhlh1/2, however, has an unique basic domain containing a highly charged arginine-rich R6 domain immediately preceding the canonical basic domain. The expanded basic domain of Nhlh1/2 was speculated to enable them to bind to a unique set of regulatory elements (Begley et al., 1992; Brown and Baer, 1994; Brown et al., 1992), although the

importance of the R6 domain had not been tested. Our result on the requirement of R6 domain for Robo3 induction suggests that Nhlh1/2 activates Robo3 via binding to specific regulatory motifs that are unlikely to be regulated by other families of bHLH TFs. The HLH domain of Nhlh1/2 is also indispensable for Robo3 induction, as the Nhlh1 mutant allele lacking the HLH domain fails to activate Robo3. Previous in vitro studies have shown that mouse and human Nhlh1/2 could interact with a range of cofactors, including class I bHLH proteins (E12, E47), LIM-only proteins (Lmo1-4), Signal Transducer and Activator of Transcription 3 (STAT3), or even homodimerize (Aoyama et al., 2005; Bao et al., 2000; Brown and Baer, 1994; Fox and Good, 2008; Isogai et al., 2011; Krüger et al., 2004; Manetopoulos et al., 2003; Uittenbogaard et al., 1999). Heterodimerization between Nhlh1 and Nhlh2, however, is not needed for Robo3 induction in vivo, because Nhlh1 and Nhlh2 single mutant shows normal commissure formation. We envisage that Nhlh1- and Nhlh2-containing transcriptional complexes function redundantly, by utilizing the same, or different binding sites on the promoter/enhancer, for Robo3 induction. Nhlh1/2 have been suggested to act either as an activator or as a repressor (Good and Braun, 2013; Isogai et al., 2011; Krüger et al., 2004; Manetopoulos et al., 2003; Wankhade and Good, 2011), perhaps depending on the nature of cofactors they associate with. Here we have shown by using VP16- and EnR-fusions that Nhlh1/2 serve as activators in respect of Robo3 induction.

Nhlh1 and Nhlh2, determine the axon projection laterality of commissural neurons

Nhlh1 and Nhlh2 are expressed in post-mitotic immature neurons (Begley et al., 1992; Gobel et al., 1992; Murdoch et al., 1999), therefore, are expected to regulate early neuronal differentiation. However, their function in neural development has remained

largely obscure, perhaps in part due to their highly overlapping expression patterns and functional redundancy. In the single mutant, the only defect found during CNS development is the migration of gonadotropin hormone releasing hormone (GnRH) neurons in Nhlh2 KO (Krüger et al., 2004). Double KO of Nhlh1/2 have been generated and analyzed (Krüger and Braun, 2002; Krüger et al., 2004; Schmid et al., 2007). Surprisingly, although these mice die at birth (Cogliati et al., 2002; Krüger and Braun, 2002), only two defects have been found so far: one an exacerbated GnRH migration defect, and second a migration defect of PN neurons causing lateralized PN positions (Krüger et al., 2004; Schmid et al., 2007). Neither of these defects could account for the perinatal lethality, suggesting defects yet undiscovered.

By generating Nhlh1/2 deficient mice, we found that they lack ventral commissures from the spinal cord to the midbrain. The commissural defect provides a satisfactory explanation to the perinatal lethality of these mice, as de-synchronization of the respiratory oscillator owing to disrupted commissural connections in the hindbrain preBötzinger complex was suggested as a cause for perinatal death in Robo3 KO mice (Bouvier et al., 2010; Sabatier et al., 2004). The PN migration defect, also can be explained by a lack of attraction of PN leading processes to the FP due to marked reduction of Robo3 in PN neurons, therefore, failing to pull the PN neuronal soma close to the midline. Besides the obvious lack of ventral commissures, other major axon tracts such as the motor axons appear normal at a gross level (Figure 7, data not shown), although a fine-grained analysis of non-commissural axon projections still await future investigations as the expression patterns of Nhlh1/2 extend beyond that of Robo3.

We think that in the commissural system, Nhlh1/2 might be dedicated to control Robo3 expression and the absence of commissures in the double mutant is chiefly due

to the down-regulation of Robo3. The commissure-less phenotype in the Nhlh1/2 double mutant and Robo3 KO are remarkably similar in details (Marillat et al., 2004; Sabatier et al., 2004; Tamada et al., 2008). For example, the spinal commissural axons appeared normal in the dorsal half, but deflected from the midline upon entering the ventral half of the spinal cord (Fig. 7) (Sabatier et al., 2004). Furthermore, we have also provided evidence that the generation and the initial axon extension of commissural neurons are not affected in the double mutant.

Are Nhlh1/2 sufficient to confer contralateral axon projection? In the midbrain, majority of neurons accessible to EP labeling at E11.5 are ipsilaterally-projecting neurons (Inamata and Shirasaki, 2014). We found that a portion of them could be driven to project contralaterally upon forced expression of Nhlh1/2. This is supported by similar observations in the hindbrain. The sufficiency of Nhlh1/2 in instructing axon laterality, however, should be reached with caution. Zelina et al. (2014) showed that mouse Robo3, via binding to DCC, promote axon extension to FP by potentiating Netrin-1 responsiveness of commissural axons, which implies that both Robo3 and DCC need to be present for neurons to respond to Netrin-1. We have found no evidence so far that Nhlh1/2 could induce DCC expression (Zhu, unpublished data), which is reflected by the un-altered DCC levels in the double mutant. It is reasonable to assume that the ectopic contralateral projection driven by Nhlh1/2 force-expression might come from DCC-expressing ipsilateral neurons. Indeed, immunohistochemistry on midbrain samples at E14.5 showed that DCC was expressed in the midbrains including some of the EP cells (Zhu, unpublished data). It might be fair to say that Nhlh1/2 are sufficient to induce contralateral axon projection depending on cellular contexts.

A global regulatory mechanism for all FP-crossing commissural axons

Whether the specification of shared traits in disparate classes of neurons are determined by common regulatory mechanism or are separately regulated is a fundamental yet unresolved neurodevelopmental issue. The same neurotransmitter phenotype appears to be regulated by different gene regulatory programs acting on distinct cis-regulatory elements in different neuronal types (Hobert and Kratsios, 2019; Lai et al., 2016; Serrano-Saiz et al., 2013). Contralateral axon projection is a common trait imposed during a transient period of development upon commissural neurons that are highly heterogenous in terms of their neurotransmitter types, synaptic targets, developmental origins, and functionality (Chédotal, 2014; Tulloch et al., 2019). Take the mouse spinal cord for example, 8 out of 13 cardinal spinal classes (dI1, dI3, dI4, dI5, dI6, dILA, dILB, V0), contain a mixture of contralateral and ipsilateral projecting neurons (Alaynick et al., 2011; Lai et al., 2016; Tulloch et al., 2019). Prior to this study, no common regulatory mechanism has been found to control Robo3 expression and commissural axon projection (Chédotal, 2014; Friocourt and Chédotal, 2017). A few TFs have been implicated in Robo3 induction, but every one of them functions only in specific neuron classes. Lhx2, the only TF confirmed to be an immediate regulator, is responsible for Robo3 expression specifically in dI1 spinal neurons (Ding et al., 2012; Wilson et al., 2008). Accordingly, we found that forced expression of Lhx2 did not induce Robo3 in the rhombic lip and the midbrain, suggesting that key cofactors required for Lhx2 to induce Robo3 are missing. Homeobox domain TF, Dbx1, expressed in the neural progenitor zones, was found to regulate Robo3 expression in the midbrain, and the interneurons in hindbrain preBötzinger complex (Bouvier et al., 2010;

Inamata and Shirasaki, 2014), most likely as an early cell fate determinant. Dbx1 may operate via its downstream target Evx2 to control Robo3 expression in the midbrain (Inamata and Shirasaki, 2014).

Our study has found that Nhlh1/2 comprise a global regulatory mechanism that controls the contralateral axon projections (Robo3 expression) common to all FP-crossing commissural neurons. Robo3 protein expression level in the double mutant is barely detectable from the spinal cord to the midbrain, suggesting that transcription of Robo3 across heterogenous commissural neuron classes is predominantly driven by Nhlh1/2-mediated mechanism. Therefore, the TFs previously found to function in specific neuron classes most likely operate via Nhlh1/2. Lhx2, for example, might form a complex with Nhlh1/2, directly or via intermediary cofactors, as a result of which promotes robo3 transcription. Indeed, in silico analysis showed that there is a Lhx2 binding site adjacent to the Nhlh1/2 binding site in the highly conserved promoter region (Zhu, unpublished). Dbx1, as a distant upstream regulator, on the other hand, may induce Robo3 expression via activating the expression of Nhlh1/2. We tested this idea by electroporating Dbx1 into the midbrain and found that concomitant with the induction of Robo3 as previously shown (Inamata and Shirasaki, 2014), Nhlh2 was indeed induced (Supplemental Figure 16), supporting this idea.

A recent study showed that the tightly regulated spatial and temporal patterns of Robo3 distribution is highly conserved in the CNS across divergent vertebrate species (Friocourt et al., 2019). They suggest that the deployment of Robo3 to promote contralateral axon projections across the FP might be a strategy that emerged during early vertebrate evolution. The conservation of Robo3 in vertebrates raises the possibility that Robo3 might be under the control of conserved gene regulatory

programs. Indeed, a phylogenetic analysis showed that Nhlh1/2 emerged in the vertebrates and are present throughout the vertebrate lineage (Zhu, unpublished), suggesting that regulation of Robo3 expression by Nhlh1/2 might be conserved. Hence, this evolutionarily ancient regulatory unit might be recruited and incorporated into the multitude of regulatory programs that control the diversification of neuron classes.

Specificity of commissural neuron fate determination

There is a gross-level spatial and temporal correlation between the expression pattern of Nhlh1/2 and Robo3 from the spinal cord to the midbrain. Furthermore, a recent RNA-seq study showed that Nhlh2 is enriched in the Robo3-positive spinal neurons (Tulloch et al., 2019). However, Nhlh1/2 are unlikely to be the sole determinant of commissural fate, because their expression pattern appears wider than that of Robo3. For example, in the spinal cord, Nhlh1/2 are expressed, albeit at lower levels, in what appears to be V1 and V2 spinal neurons which are Robo3-negative ipsilateral neurons (Alaynick et al., 2011; Tulloch et al., 2019), and at an earlier stage in the young motor neurons (Murdoch et al., 1999). We propose that the specificity of Robo3 expression might be determined by a combination of two levels of regulation. The first is the total amount of Nhlh1 and Nhlh2. The second is an additional layer of Robo3 regulation, via activators or repressors, most probably converging on Nhlh1/2. As discussed above, a range of molecules have been found to be able to interact with Nhlh1/2 in vitro, such as class I bHLH E proteins (E12, E47) and LIM-only proteins (Lmo1-4) (Aoyama et al., 2005; Bao et al., 2000; Brown and Baer, 1994; Isogai et al., 2011; Krüger et al., 2004; Manetopoulos et al., 2003; Uittenbogaard et al., 1999).

There are precedents showing that E proteins and Lmo proteins are capable of fine tuning the gene regulatory mechanisms mediated by class II bHLH proteins (Joshi et al., 2009; Le Dreau et al., 2018). It would be of future interest to interrogate whether any of these potential cofactors may modulate the activity of Nhlh1/2 in the specification of commissural neuronal fate. The intersection of the global mechanism uncovered here with neuron subtype-specific regulatory mechanisms should ultimately determine the specific and the balanced production of the contralateral- versus ipsilateral-projection neurons to achieve optimized outcomes at the neural circuitry level.

MATERIALS and METHODS

DNA constructs

Expression constructs pCAG-EGFP and pCAG-mCherry have been described before (Hatanaka and Murakami, 2002; Tanaka et al., 2009; Zhu et al., 2015). pCAG-nls-EGFP was a kind gift from Dr. Yasuto Tanabe (Kyoto University, Japan). Full-length (fl) Nnlh1 and Nhlh2 expression constructs were constructed by PCR amplification of the coding sequences of Nhlh1 (GenBank accession: NM_010916) and Nhlh2 (GenBank accession: NM_178777) from mouse E11.5 brain cDNA. The PCR products were cloned into a pCAGGS vector with a multiple cloning site inserted (Nishida et al., 2011; Niwa et al., 1991) to generate pCAG-Nhlh1-fl and pCAG-Nhlh2-fl. The PCR products were also cloned into a pCAG-2HA plasmid which contains the pCAGGS backbone with two Hemagglutinin (HA) tags. This resulted in the generation of fusion proteins of Nhlh1 and Nhlh2 with two HA tags at their N-termini. The HA fused or non-fused versions of Nhlh1 and Nhlh2 were confirmed to be equivalent in inducing Robo3 expression (data not shown). To produce Nhlh1- and

Nhlh2-VP16 fusion proteins, the VP16 and EnR coding sequences were excised from pCS2+NLSVP16AD and pCS2+EnR plasmids (kind gifts from Dr. Masahiko Hibi, Nagoya University, Japan) (Shimizu et al., 2002), respectively, and cloned into pCAG-Nhlh1-fl and pCAG-Nhlh2-fl at 5' to and in frame with Nhlh1 and Nhlh2 coding sequences. To construct the pCAG-bHLH1-VP16 and pCAG-bHLH2-VP16 constructs, the bHLH domains (excluding the R6) of Nhlh1 and Nhlh2 were PCR amplified with forward primer, 5'ATCTCGAGGCCACGGCCAAGT3', for both Nhlh1 and Nhlh2, and reverse primers 5'ATAGCGGCCGCTCAGACGTCCAGCA3' for Nhlh1 and 5'ATAGCGGCCGCCTACACGTCCAGGA3' for Nhlh2. To construct pCAG-R6-bHLH1-VP16 and pCAG-R6-bHLH2-VP16, the R6-bHLH domains, from Nhlh1 and Nhlh2, were PCR amplified with forward primers 5'CGCTCGAGCACTTGAGTCGTGAG3' and 5'ATCTCGAGCAGCTGAGCCGCGAA3', for Nhlh1 and Nhlh2, respectively, and the same reverse primers as above. The PCR fragments were cut with XhoI and NotI, and were subcloned into XhoI and NotI digested pCAG-Nhlh1-VP16 and pCAG-Nhlh2-VP16 plasmids to replace the full-length Nhlh1 and Nhlh2, respectively. The Dbx1 expression construct (pCAG-Dbx1-ires-nlsEGFP) was a kind gift from Dr. Alexandra Pierani (INSERM, France) (Arai et al., 2019). All the cloned expression constructs were confirmed by sequencing.

Constructs for generating riboprobes to detect Robo3, Nhlh1, Nhlh2, Netrin-1 were made using the pGEM-T Easy vector system (Promega) by PCR amplification from E11.5 mouse brain cDNA with the following primer pairs: 5'ACAGCAGCCTATCTAGGCCA3' and 5'TCTGGTATTCAGTGATGACCCC3' for

Robo3, 5'TGTTCAGCCACAAGCTGC3' and 5'GCGCTCCTCACGACTCAA3' for Nhlh1, 5'CTGCCAAAGGCGACTCAT3' and 5'AGACGGGGTGTTTTTGGA3' for Nhlh2, and 5'CTTCCTCACCGACCTCAATAAC3' and 5'TAGAGCTCCATGTTGAATCTGC3' for Netrin-1. Sonic hedgehog (Shh) ISH probe was a kind gift from Dr. Toshihiko Shiroishi and Dr. Tomoko Sagai (National Institute of Genetics, Japan) (Sagai et al., 2019).

For generating sgRNA for gene editing in fertilized eggs, oligonucleotide pairs were annealed and cloned into BbsI digested pX330 (Addgene, Plasmid#42230): for Nhlh1-sg1, 5'CACCGGACCGGGCCCCGATGGTGC3' and 5'AAACGCACCATCGGGGCCCGGTCC3'; for Nhlh1-sg2, 5'CACCGCTAGGTTGAAGGCTTCCACG3' and 5'AAACCGTGGAAGCCTTCAACCTAGC3'; for Nhlh2-sg1, 5'CACCGCGAAGAAAAGCGCCGCCGC3' and 5'AAACGCGGCGGCGCTTTTCTTCGC3'; for Nhlh2-sgRNA2, 5'CACCGTTCTTGTCCGGAGGCAGCGT3' and 5'AAACACGCTGCCTCCGGACAAGAAC3'. The target regions are underlined.

Generation of Nhlh1 and Nhlh2 mutant mice

The CRISPR/Cas9 guide sequences for Nhlh1 and Nhlh2 genes were selected using CRISPOR (http://crispor.tefor.net) and CRISPRdirect (http://crispr.dbcls.jp) webtools (Supplemental Fig. 7A, B). The sgRNAs were synthesized as reported previously (Ajima et al., 2017). B6C3F1 (C57BL/6N X C3H/HeN) female mice were super-ovulated and mated with B6C3F1 males, and fertilized eggs were collected from

oviducts. The 50 ng/μl synthesized sgRNAs and 100 ng/μl TrueCut Cas9 protein v2 (Invitrogen) were premixed in Opti-MEM (Thermo Fisher Scientific) and electroporated into fertilized eggs using CUY21EDIT II electroporator and LF501PT1-10 platinum plate electrode (BEX Co. Ltd.) following the method reported previously (Hashimoto and Takemoto, 2015). The electroporated zygotes were cultured in KSOM (Millipore) at 37°C under 5% CO_2 until the two-cell stage after 1.5 days. Thereafter, 20 to 32 two-cell stage embryos were transferred into the uterus of pseudo-pregnant MCH females at 0.5 days post coitum. Founder mice were screened for edited Nhlh1 and Nhlh2 alleles which were subsequently sequenced to obtain the precise nature of the edited alleles. Two founder lines were then chosen for breeding, backcrossing and analyses (Supplemental Fig. 7C, D).

Animals

For expression studies with ISH and in utero EP, timed pregnant ICR mice (Nihon SLC, Shizuoka, Japan) were used. Noon of the day on which a vaginal plug was detected was designated as embryonic day (E) 0.5. Nhlh1 and Nhlh2 mutant mouse lines, initially on a B6C3F1 hybrid background, were backcrossed to C57BL/6J for at least two to five generations before phenotype analyses. Double and single heterozygotic colonies were maintained. To generate double homozygotic embryos, double heterozygotic male and female mice were crossed. Genotyping were performed on tail lysis using the following primers. For Nhlh1 mutant, 5'AGTCGGGCTTTAGCGACTGT3' and 5'GCGAAGGCTAGGTTGAAGG3' were used; and for Nhlh2 mutant 5'AAACTACTACCCACGCTGCC3', 5'CCACTACTCCTTGCAAATCAAGA3',

5’GACTAGAAAGAACAGGCTGCAAA3’, and

5’AGACGTTCTTGTCCGGAGTAG3’ were used. All animal maintenance and manipulations were carried out in accordance with the Guidelines for the Welfare and Use of Laboratory Animals of the National Institute of Genetics, Japan.

In utero electroporation

In utero EP was performed essentially as previously described (Zhu et al., 2020) with some modifications. The pregnant mice were anesthetized with a combination of isoflurane (1.0% in air) and Pentobarbital Sodium (Somnopentyl, Kyoritsu Seiyaku Corporation, Tokyo, Japan, 80 mg/kg body weight). The uterus was exposed after abdominal incision and approximately 2 μl of plasmid was injected into the IV ventricle or the cerebral aqueduct of E12.5 or E11.5 embryos. Five square electric pulses (30V, 50 ms duration at 200 ms intervals) were applied using a forceps-type electrode (CUY650P5 or CUY650P2, Nepa Gene, Japan) connected to a square-pulse generator (CUY21, BEX, Japan).

Tissue processing and sectioning

Pregnant mice were killed by cervical dislocation and embryos were taken out from the uterus. Mouse brainstems were dissected out in phosphate-buffered saline (PBS, pH7.4) and fixed in 4% paraformaldehyde (PFA, 0.01 M PBS) at 4°C for 6-7 hr. The tissues were then cryo-protected in 30% sucrose (in PBS) overnight at 4°C and embedded in O.C.T compound (Sakura FineTek, Japan). Frozen sections of 20 μm thickness were obtained with a cryostat (Leica CM3050S).

In situ hybridization on sections

Tissue sections were pre-hybridized at 65°C for 2 hr in hybridization buffer comprised of: 50% Formamide (deionized and nuclease tested, Nacalai tesque), 1.3x SSC, 1xDenhardt's Solution (Wako), 0.1mg/ml yeast tRNA and 10% (w/v) Dextran Sulphate (M.W.500000, Millipore). The sections were then incubated with hybridization buffer containing 1.5μg/ml of anti-sense riboprobe at 65°C overnight. The next day, sections were washed twice at 65°C with formamide wash buffer (50% Formamide, 1xSSC, 0.1% Tween-20), and then twice at room temperature (RT) with 1xMABT (100mM Maleic Acid, 150mM NaCl, 0.1% Tween-20). Blocking was performed in 1xMABT with 2% Blocking Reagents (Roche) and 10% donkey serum (Sigma) for 1 hr at RT, and reacted with anti-DIG-AP Fab fragments (1:1500, Roche) in the blocking solution at 4°C overnight. The next day, slides were washed three times in 1xMABT and rinsed once in NTMT solution (0.1M Tris-HCl pH9.5, 0.1M NaCl, 0.05M MgCl2, 0.1% Tween-20), and then color developing was carried out in NTMT containing NBT (100ug/ml) and BCIP (50ug/ml).

Immunohistochemistry

IHC was performed as previously described (Zhu et al., 2015). The sections were blocked with 10% donkey serum (Sigma) in PBSTx (0.2% Triton X-100) for 1 hr at RT followed by incubation with primary antibodies at 4°C overnight. After washing with PBSTx, the sections were then incubated with the secondary antibodies at RT for 2 hr. Slides were counter-stained with 0.03% 4,6-diamidino-2-phenylindole (DAPI, Nacalai tesque). The primary antibodies used were: rabbit anti-Barhl1 polyclonal antibody (Atlas Antibodies, HPA004809, Sigma, 1:500), goat anti-Robo3 polyclonal antibody

(R&D Systems, AF3076, 1:200), goat anti-Tag1 polyclonal antibody (R&D Systems, AF4439, 1:500), mouse anti-Neurofilament-160KD monoclonal antibody (clone: RMO-270, Zymed, 13-0700, 1:500), rat anti-L1CAM monoclonal antibody (clone 324, Chemicon, MAB5272, 1:400), goat anti-DCC polyclonal antibody (Santa Cruz Biotechnology, sc-6535, 1:200), rabbit anti-FoxP2 polyclonal antibody (abcam, ab16046, 1:1000), mouse anti-Brn3a monoclonal antibody (clone: 5A3.2, Millipore, MAB1585, 1;200), chick anti-GFP polyclonal antibody (abcam, ab13970, 1:1500). The secondary antibodies used were Cy3-donkey anti-rabbit IgG (Jackson ImmunoResearch, 1:300) for Barhl1, FoxP2 antibodies, Cy3-donkey anti-goat IgG (Jackson ImmunoResearch, 1:300) for Robo3, Tag1, DCC antibodies, Cy3-donkey anti-mouse IgG (Jackson ImmunoResearch, 1:300) for Neurofilament, Brn3a antibodies, Cy3-donkey anti-rat IgG (Jackson ImmunoResearch, 1:300) for an L1CAM antibody, Alexa Fluor 488-donkey anti-chick IgY (Jackson ImmunoResearch, 1:400) for a GFP antibody.

Transcriptional Factor binding site analysis

Promoter sequences of mouse, human, rabbit, cow, ferret and opossum Robo3 were extracted using the UCSC genome browser (http://genome.ucsc.edu). The transcriptional start site (TSS) information were obtained from the Eukaryotic Promoter Database (EPD, https://epd.epfl.ch//index.php) (Perier et al., 2000). The Nhlh1 and Nhlh2 binding site position frequency matrices (PFM) were downloaded from JASPAR (http://jaspar.genereg.net) (Castro-Mondragon et al., 2022). Using the FIMO tool from the MEME suite (https://meme-suite.org/meme/, Bailey et al., 2015; Grant et al., 2011), the promoter region of mouse Robo3 was scanned for Nhlh1 and Nhlh2 binding sites

with their respective PFM from JASPAR. Only regions identified to be bound by both Nhlh1 and Nhlh2 were illustrated in Figure 1. Phylogenetic foot printing was performed by using the mVISTA tool in VISTA (http://genome.lbl.gov/vista) (Brudno et al., 2003; Frazer et al., 2004). Conservation parameters were set to be: minY 50%, minID 70%, min Length 100 bases.

Image acquisition and processing

Fluorescence images on sections or flat-mounted brainstems were captured with a CCD camera (Axiocam, Zeiss) attached to an upright microscope (BX-60, Olympus) at 1296x1030 pixel resolution. Objective lens used were: 2x Plan Apo with numerical aperture (NA) 0.08 (Olympus), 4x UPlan Apo with NA 0.16 (Olympus), 10x UPlan Apo with NA 0.40 (Olympus) and 20x UPlan Apo with NA 0.70 (Olympus). All bright field images on ISH sections, as well as some fluorescence images were captured with an All-in-one Fluorescence Microscope (BZ-X700, Keyence) with an objective lens of CFI 10x Plan Apo Lamda, NA 0.45 (Nikon). Adobe Photoshop CC was used to adjust contrast and brightness of images and to assemble figures.

Quantification and statistical analysis

For quantifying the commissural index in the electroporated midbrains, fluorescence images of the whole-mounted brainstems were imported into ImageJ (NIH, http://imagej.nih.gov/ij/). An ROI of defined size over the ipsilateral extending axons, the contralateral extending axons and a background region on the sample were measured for its mean fluorescence level denoted as F_i, F_c, and F_b, respectively. The commissural index was calculated as $(F_c-F_b)/(F_i-F_b)$. For quantifying the commissural

index in the electroporated hindbrains, fluorescence images of the hindbrain sections after IHC were imported into ImageJ. An ROI of defined size over a region just below the rhombic lip, the FP region, and a background region on the sample were measured for its mean fluorescence level denoted as F_{ep}, F_{fp}, and F_b, respectively. The commissural index was calculated as $(F_{fp}-F_b)/(F_{ep}-F_b)$. The quantified data were represented by scatter plots with median and upper and lower quartiles indicated and statistical analyses were performed by Mann-Whitney U test using Prism 8 (GraphPad). To quantify the number of Brn3a positive neurons on the spinal cord samples, the number of Brn3a signal positive cells were manually counted on 2-3 sections for each sample and subsequently averaged. This was done for all the samples on spinal cord sections of approximately equivalent axial levels. The data points were represented on a scatter plot using Microsoft excel.

ACKNOWLEDGEMENTS: The authors thank Ms. Noriko Yamatani, Ms. Mami Yokoyama, and Ms. Sayuri Noguchi for their technical assistance, Dr. Alexandra Pierani for Dbx1 expression construct, Dr. Yasuto Tanabe for nls-EGFP expression construct, Dr. Masahiko Hibi for VP16 and EnR containing plasmids, Drs. Toshihiko Shiroishi and Tomoko Sagai for Shh riboprobe, Drs. Fujio Murakami and Yash Hiromi for critical reading of the manuscript. This study was funded by Grants-in-Aid for Scientific Research from the Ministry of Education, Culture, Science and Technology, Japan, contract grant nos: 16K07010, 20K06865 (to YZ), 20H03345 (to TH).

AUTHOR CONTRIBUTIONS: YZ conceived the study. AM and YZ designed and conducted the experiments, analyzed data and wrote the manuscript. RA and YS

generated the mutant mice. TH contributed materials and advices. YZ and TH provided funding. All authors read and approved the manuscript.

DECLARATION OF INTERESTS: The authors declare no competing interests.

REFERENCES

Ajima, R., Suzuki, E., and Saga, Y. (2017). Pofut1 point-mutations that disrupt O-fucosyltransferase activity destabilize the protein and abolish Notch1 signaling during mouse somitogenesis. PLoS One *12*, e0187248.

Alaynick, W.A., Jessell, T.M., and Pfaff, S.L. (2011). SnapShot: spinal cord development. Cell *146*, 178-178 e171.

Altman, J., and Bayer, S.A. (1987). Development of the precerebellar nuclei in the rat: IV. The anterior precerebellar extramural migratory stream and the nucleus reticularis tegmenti pontis and the basal pontine gray. J Comp Neurol *257*, 529-552.

Aoyama, M., Ozaki, T., Inuzuka, H., Tomotsune, D., Hirato, J., Okamoto, Y., Tokita, H., Ohira, M., and Nakagawara, A. (2005). LMO3 interacts with neuronal transcription factor, HEN2, and acts as an oncogene in neuroblastoma. Cancer Res *65*, 4587-4597.

Arai, Y., Cwetsch, A.W., Coppola, E., Cipriani, S., Nishihara, H., Kanki, H., Saillour, Y., Freret-Hodara, B., Dutriaux, A., Okada, N., *et al.* (2019). Evolutionary Gain of Dbx1 Expression Drives Subplate Identity in the Cerebral Cortex. Cell Rep *29*, 645-658 e645.

Bai, G., Chivatakarn, O., Bonanomi, D., Lettieri, K., Franco, L., Xia, C., Stein, E., Ma, L., Lewcock, J.W., and Pfaff, S.L. (2011). Presenilin-dependent receptor processing is required for axon guidance. Cell *144*, 106-118.

Bailey, T.L., Johnson, J., Grant, C.E., and Noble, W.S. (2015). The MEME Suite. Nucleic

Acids Res *43*, W39-49.

Bao, J., Talmage, D.A., Role, L.W., and Gautier, J. (2000). Regulation of neurogenesis by interactions between HEN1 and neuronal LMO proteins. Development *127*, 425-435.

Barber, M., Di Meglio, T., Andrews, W.D., Hernandez-Miranda, L.R., Murakami, F., Chédotal, A., and Parnavelas, J.G. (2009). The role of Robo3 in the development of cortical interneurons. Cereb Cortex *19 Suppl 1*, i22-31.

Begley, C.G., Lipkowitz, S., Gobel, V., Mahon, K.A., Bertness, V., Green, A.R., Gough, N.M., and Kirsch, I.R. (1992). Molecular characterization of NSCL, a gene encoding a helix-loop-helix protein expressed in the developing nervous system. Proc Natl Acad Sci U S A *89*, 38-42.

Belle, M., Godefroy, D., Dominici, C., Heitz-Marchaland, C., Zelina, P., Hellal, F., Bradke, F., and Chédotal, A. (2014). A simple method for 3D analysis of immunolabeled axonal tracts in a transparent nervous system. Cell Rep *9*, 1191-1201.

Bertrand, N., Castro, D.S., and Guillemot, F. (2002). Proneural genes and the specification of neural cell types. Nat Rev Neurosci *3*, 517-530.

Borst, J.G., and Soria van Hoeve, J. (2012). The calyx of Held synapse: from model synapse to auditory relay. Annu Rev Physiol *74*, 199-224.

Bouvier, J., Thoby-Brisson, M., Renier, N., Dubreuil, V., Ericson, J., Champagnat, J., Pierani, A., Chédotal, A., and Fortin, G. (2010). Hindbrain interneurons and axon guidance signaling critical for breathing. Nat Neurosci *13*, 1066-1074.

Brown, L., and Baer, R. (1994). HEN1 encodes a 20-kilodalton phosphoprotein that binds an extended E-box motif as a homodimer. Mol Cell Biol *14*, 1245-1255.

Brown, L., Espinosa, R., 3rd, Le Beau, M.M., Siciliano, M.J., and Baer, R. (1992). HEN1 and HEN2: a subgroup of basic helix-loop-helix genes that are coexpressed in a human

neuroblastoma. Proc Natl Acad Sci U S A *89*, 8492-8496.

Brudno, M., Do, C.B., Cooper, G.M., Kim, M.F., Davydov, E., Program, N.C.S., Green, E.D., Sidow, A., and Batzoglou, S. (2003). LAGAN and Multi-LAGAN: efficient tools for large-scale multiple alignment of genomic DNA. Genome Res *13*, 721-731.

Castro-Mondragon, J.A., Riudavets-Puig, R., Rauluseviciute, I., Lemma, R.B., Turchi, L., Blanc-Mathieu, R., Lucas, J., Boddie, P., Khan, A., Manosalva Perez, N.*, et al.* (2022). JASPAR 2022: the 9th release of the open-access database of transcription factor binding profiles. Nucleic Acids Res *50*, D165-D173.

Charron, F., Stein, E., Jeong, J., McMahon, A.P., and Tessier-Lavigne, M. (2003). The morphogen sonic hedgehog is an axonal chemoattractant that collaborates with netrin-1 in midline axon guidance. Cell *113*, 11-23.

Chédotal, A. (2011). Further tales of the midline. Curr Opin Neurobiol *21*, 68-75.

Chédotal, A. (2014). Development and plasticity of commissural circuits: from locomotion to brain repair. Trends Neurosci *37*, 551-562.

Chédotal, A. (2019). Roles of axon guidance molecules in neuronal wiring in the developing spinal cord. Nat Rev Neurosci *20*, 380-396.

Cogliati, T., Good, D.J., Haigney, M., Delgado-Romero, P., Eckhaus, M.A., Koch, W.J., and Kirsch, I.R. (2002). Predisposition to arrhythmia and autonomic dysfunction in Nhlh1-deficient mice. Mol Cell Biol *22*, 4977-4983.

Comer, J.D., Alvarez, S., Butler, S.J., and Kaltschmidt, J.A. (2019). Commissural axon guidance in the developing spinal cord: from Cajal to the present day. Neural Dev *14*, 9.

Comer, J.D., Pan, F.C., Willet, S.G., Haldipur, P., Millen, K.J., Wright, C.V., and Kaltschmidt, J.A. (2015). Sensory and spinal inhibitory dorsal midline crossing is independent of Robo3. Front Neural Circuits *9*, 36.

Dennis, D.J., Han, S., and Schuurmans, C. (2019). bHLH transcription factors in neural development, disease, and reprogramming. Brain Res *1705*, 48-65.

Di Meglio, T., Nguyen-Ba-Charvet, K.T., Tessier-Lavigne, M., Sotelo, C., and Chédotal, A. (2008). Molecular mechanisms controlling midline crossing by precerebellar neurons. J Neurosci *28*, 6285-6294.

Dillon, A.K., Fujita, S.C., Matise, M.P., Jarjour, A.A., Kennedy, T.E., Kollmus, H., Arnold, H.H., Weiner, J.A., Sanes, J.R., and Kaprielian, Z. (2005). Molecular control of spinal accessory motor neuron/axon development in the mouse spinal cord. J Neurosci *25*, 10119-10130.

Ding, Q., Joshi, P.S., Xie, Z.H., Xiang, M., and Gan, L. (2012). BARHL2 transcription factor regulates the ipsilateral/contralateral subtype divergence in postmitotic dI1 neurons of the developing spinal cord. Proc Natl Acad Sci U S A *109*, 1566-1571.

Dodd, J., Morton, S.B., Karagogeos, D., Yamamoto, M., and Jessell, T.M. (1988). Spatial regulation of axonal glycoprotein expression on subsets of embryonic spinal neurons. Neuron *1*, 105-116.

Dominici, C., Moreno-Bravo, J.A., Puiggros, S.R., Rappeneau, Q., Rama, N., Vieugue, P., Bernet, A., Mehlen, P., and Chédotal, A. (2017). Floor-plate-derived netrin-1 is dispensable for commissural axon guidance. Nature *545*, 350-354.

Duncan, M.K., Bordas, L., Dicicco-Bloom, E., and Chada, K.K. (1997). Expression of the helix-loop-helix genes Id-1 and NSCL-1 during cerebellar development. Dev Dyn *208*, 107-114.

Fan, M.J., and Sokol, S.Y. (1997). A role for Siamois in Spemann organizer formation. Development *124*, 2581-2589.

Fazeli, A., Dickinson, S.L., Hermiston, M.L., Tighe, R.V., Steen, R.G., Small, C.G.,

Stoeckli, E.T., Keino-Masu, K., Masu, M., Rayburn, H., *et al.* (1997). Phenotype of mice lacking functional Deleted in colorectal cancer (Dcc) gene. Nature *386*, 796-804.

Fox, D.L., and Good, D.J. (2008). Nescient helix-loop-helix 2 interacts with signal transducer and activator of transcription 3 to regulate transcription of prohormone convertase 1/3. Mol Endocrinol *22*, 1438-1448.

Frazer, K.A., Pachter, L., Poliakov, A., Rubin, E.M., and Dubchak, I. (2004). VISTA: computational tools for comparative genomics. Nucleic Acids Res *32*, W273-279.

Friocourt, F., and Chédotal, A. (2017). The Robo3 receptor, a key player in the development, evolution, and function of commissural systems. Dev Neurobiol *77*, 876-890.

Friocourt, F., Kozulin, P., Belle, M., Suarez, R., Di-Poi, N., Richards, L.J., Giacobini, P., and Chédotal, A. (2019). Shared and differential features of Robo3 expression pattern in amniotes. J Comp Neurol *527*, 2009-2029.

Gobel, V., Lipkowitz, S., Kozak, C.A., and Kirsch, I.R. (1992). NSCL-2: a basic domain helix-loop-helix gene expressed in early neurogenesis. Cell Growth Differ *3*, 143-148.

Good, D.J., and Braun, T. (2013). NHLH2: at the intersection of obesity and fertility. Trends Endocrinol Metab *24*, 385-390.

Good, D.J., Porter, F.D., Mahon, K.A., Parlow, A.F., Westphal, H., and Kirsch, I.R. (1997). Hypogonadism and obesity in mice with a targeted deletion of the Nhlh2 gene. Nat Genet *15*, 397-401.

Goulding, M. (2009). Circuits controlling vertebrate locomotion: moving in a new direction. Nat Rev Neurosci *10*, 507-518.

Grant, C.E., Bailey, T.L., and Noble, W.S. (2011). FIMO: scanning for occurrences of a given motif. Bioinformatics *27*, 1017-1018.

Haire, M.F., and Chiaramello, A. (1996). Transient expression of the basic helix-loop-helix protein NSCL-2 in the mouse cerebellum during postnatal development. Brain Res Mol Brain Res *36*, 174-178.

Hashimoto, M., and Takemoto, T. (2015). Electroporation enables the efficient mRNA delivery into the mouse zygotes and facilitates CRISPR/Cas9-based genome editing. Sci Rep *5*, 11315.

Hatanaka, Y., and Murakami, F. (2002). In vitro analysis of the origin, migratory behavior, and maturation of cortical pyramidal cells. J Comp Neurol *454*, 1-14.

Hobert, O., and Kratsios, P. (2019). Neuronal identity control by terminal selectors in worms, flies, and chordates. Curr Opin Neurobiol *56*, 97-105.

Inamata, Y., and Shirasaki, R. (2014). Dbx1 triggers crucial molecular programs required for midline crossing by midbrain commissural axons. Development *141*, 1260-1271.

Isogai, E., Ohira, M., Ozaki, T., Oba, S., Nakamura, Y., and Nakagawara, A. (2011). Oncogenic LMO3 collaborates with HEN2 to enhance neuroblastoma cell growth through transactivation of Mash1. PLoS One *6*, e19297.

Joshi, K., Lee, S., Lee, B., Lee, J.W., and Lee, S.K. (2009). LMO4 controls the balance between excitatory and inhibitory spinal V2 interneurons. Neuron *61*, 839-851.

Kawauchi, D., Muroyama, Y., Sato, T., and Saito, T. (2010). Expression of major guidance receptors is differentially regulated in spinal commissural neurons transfated by mammalian Barh genes. Dev Biol *344*, 1026-1034.

Kawauchi, D., Taniguchi, H., Watanabe, H., Saito, T., and Murakami, F. (2006). Direct visualization of nucleogenesis by precerebellar neurons: involvement of ventricle-directed, radial fibre-associated migration. Development *133*, 1113-1123.

Keino-Masu, K., Masu, M., Hinck, L., Leonardo, E.D., Chan, S.S., Culotti, J.G., and

Tessier-Lavigne, M. (1996). Deleted in Colorectal Cancer (DCC) encodes a netrin receptor. Cell *87*, 175-185.

Kennedy, T.E., Serafini, T., de la Torre, J.R., and Tessier-Lavigne, M. (1994). Netrins are diffusible chemotropic factors for commissural axons in the embryonic spinal cord. Cell *78*, 425-435.

Kiehn, O. (2016). Decoding the organization of spinal circuits that control locomotion. Nat Rev Neurosci *17*, 224-238.

Krüger, M., and Braun, T. (2002). The neuronal basic helix-loop-helix transcription factor NSCL-1 is dispensable for normal neuronal development. Mol Cell Biol *22*, 792-800.

Krüger, M., Ruschke, K., and Braun, T. (2004). NSCL-1 and NSCL-2 synergistically determine the fate of GnRH-1 neurons and control necdin gene expression. EMBO J *23*, 4353-4364.

Lai, H.C., Seal, R.P., and Johnson, J.E. (2016). Making sense out of spinal cord somatosensory development. Development *143*, 3434-3448.

Lanuza, G.M., Gosgnach, S., Pierani, A., Jessell, T.M., and Goulding, M. (2004). Genetic identification of spinal interneurons that coordinate left-right locomotor activity necessary for walking movements. Neuron *42*, 375-386.

Laumonnerie, C., Tong, Y.G., Alstermark, H., and Wilson, S.I. (2015). Commissural axonal corridors instruct neuronal migration in the mouse spinal cord. Nat Commun *6*, 7028.

Le Dreau, G., Escalona, R., Fueyo, R., Herrera, A., Martinez, J.D., Usieto, S., Menendez, A., Pons, S., Martinez-Balbas, M.A., and Marti, E. (2018). E proteins sharpen neurogenesis by modulating proneural bHLH transcription factors' activity in an E-box-dependent manner. Elife *7*.

Manetopoulos, C., Hansson, A., Karlsson, J., Jonsson, J.I., and Axelson, H. (2003). The LIM-only protein LMO4 modulates the transcriptional activity of HEN1. Biochem Biophys Res Commun *307*, 891-899.

Marillat, V., Sabatier, C., Failli, V., Matsunaga, E., Sotelo, C., Tessier-Lavigne, M., and Chédotal, A. (2004). The slit receptor Rig-1/Robo3 controls midline crossing by hindbrain precerebellar neurons and axons. Neuron *43*, 69-79.

Moreno-Bravo, J.A., Roig Puiggros, S., Mehlen, P., and Chédotal, A. (2019). Synergistic Activity of Floor-Plate- and Ventricular-Zone-Derived Netrin-1 in Spinal Cord Commissural Axon Guidance. Neuron *101*, 625-634 e623.

Murdoch, J.N., Eddleston, J., Leblond-Bourget, N., Stanier, P., and Copp, A.J. (1999). Sequence and expression analysis of Nhlh1: a basic helix-loop-helix gene implicated in neurogenesis. Dev Genet *24*, 165-177.

Nishida, K., Nakayama, K., Yoshimura, S., and Murakami, F. (2011). Role of Neph2 in pontine nuclei formation in the developing hindbrain. Mol Cell Neurosci *46*, 662-670.

Niwa, H., Yamamura, K., and Miyazaki, J. (1991). Efficient selection for high-expression transfectants with a novel eukaryotic vector. Gene *108*, 193-199.

Okada, A., Charron, F., Morin, S., Shin, D.S., Wong, K., Fabre, P.J., Tessier-Lavigne, M., and McConnell, S.K. (2006). Boc is a receptor for sonic hedgehog in the guidance of commissural axons. Nature *444*, 369-373.

Okada, T., Keino-Masu, K., and Masu, M. (2007). Migration and nucleogenesis of mouse precerebellar neurons visualized by in utero electroporation of a green fluorescent protein gene. Neurosci Res *57*, 40-49.

Perier, R.C., Praz, V., Junier, T., Bonnard, C., and Bucher, P. (2000). The eukaryotic promoter database (EPD). Nucleic Acids Res *28*, 302-303.

Petros, T.J., Rebsam, A., and Mason, C.A. (2008). Retinal axon growth at the optic chiasm: to cross or not to cross. Annu Rev Neurosci *31*, 295-315.

Pierce, E.T. (1966). Histogenesis of the nuclei griseum pontis, corporis pontobulbaris and reticularis tegmenti pontis (Bechterew) in the mouse. An autoradiographic study. J Comp Neurol *126*, 219-254.

Placzek, M., and Briscoe, J. (2005). The floor plate: multiple cells, multiple signals. Nat Rev Neurosci *6*, 230-240.

Quina, L.A., Wang, S., Ng, L., and Turner, E.E. (2009). Brn3a and Nurr1 mediate a gene regulatory pathway for habenula development. J Neurosci *29*, 14309-14322.

Rodriguez, C.I., and Dymecki, S.M. (2000). Origin of the precerebellar system. Neuron *27*, 475-486.

Sabatier, C., Plump, A.S., Le, M., Brose, K., Tamada, A., Murakami, F., Lee, E.Y., and Tessier-Lavigne, M. (2004). The divergent Robo family protein rig-1/Robo3 is a negative regulator of slit responsiveness required for midline crossing by commissural axons. Cell *117*, 157-169.

Sadowski, I., Ma, J., Triezenberg, S., and Ptashne, M. (1988). GAL4-VP16 is an unusually potent transcriptional activator. Nature *335*, 563-564.

Sagai, T., Amano, T., Maeno, A., Ajima, R., and Shiroishi, T. (2019). SHH signaling mediated by a prechordal and brain enhancer controls forebrain organization. Proc Natl Acad Sci U S A *116*, 23636-23642.

Schmid, T., Krüger, M., and Braun, T. (2007). NSCL-1 and -2 control the formation of precerebellar nuclei by orchestrating the migration of neuronal precursor cells. J Neurochem *102*, 2061-2072.

Schmidt, E.R.E., Brignani, S., Adolfs, Y., Lemstra, S., Demmers, J., Vidaki, M., Donahoo,

A.S., Lillevali, K., Vasar, E., Richards, L.J., *et al.* (2014). Subdomain-mediated axon-axon signaling and chemoattraction cooperate to regulate afferent innervation of the lateral habenula. Neuron *83*, 372-387.

Serafini, T., Colamarino, S.A., Leonardo, E.D., Wang, H., Beddington, R., Skarnes, W.C., and Tessier-Lavigne, M. (1996). Netrin-1 is required for commissural axon guidance in the developing vertebrate nervous system. Cell *87*, 1001-1014.

Serrano-Saiz, E., Poole, R.J., Felton, T., Zhang, F., De La Cruz, E.D., and Hobert, O. (2013). Modular control of glutamatergic neuronal identity in C. elegans by distinct homeodomain proteins. Cell *155*, 659-673.

Shimizu, T., Yamanaka, Y., Nojima, H., Yabe, T., Hibi, M., and Hirano, T. (2002). A novel repressor-type homeobox gene, ved, is involved in dharma/bozozok-mediated dorsal organizer formation in zebrafish. Mech Dev *118*, 125-138.

Shinohara, M., Zhu, Y., and Murakami, F. (2013). Four-dimensional analysis of nucleogenesis of the pontine nucleus in the hindbrain. J Comp Neurol *521*, 3340-3357.

Tamada, A., Kumada, T., Zhu, Y., Matsumoto, T., Hatanaka, Y., Muguruma, K., Chen, Z., Tanabe, Y., Torigoe, M., Yamauchi, K., *et al.* (2008). Crucial roles of Robo proteins in midline crossing of cerebellofugal axons and lack of their up-regulation after midline crossing. Neural Dev *3*, 29.

Tanaka, D.H., Yanagida, M., Zhu, Y., Mikami, S., Nagasawa, T., Miyazaki, J., Yanagawa, Y., Obata, K., and Murakami, F. (2009). Random walk behavior of migrating cortical interneurons in the marginal zone: time-lapse analysis in flat-mount cortex. J Neurosci *29*, 1300-1311.

Theodorakis, K., Kyriakopoulou, K., Wassef, M., and Karagogeos, D. (2002). Novel sites of expression of the bHLH gene NSCL1 in the developing nervous system. Mech Dev

119 Suppl 1, S103-106.

Tulloch, A.J., Teo, S., Carvajal, B.V., Tessier-Lavigne, M., and Jaworski, A. (2019). Diverse spinal commissural neuron populations revealed by fate mapping and molecular profiling using a novel Robo3(Cre) mouse. J Comp Neurol *527*, 2948-2972.

Uittenbogaard, M., Peavy, D.R., and Chiaramello, A. (1999). Expression of the bHLH gene NSCL-1 suggests a role in regulating cerebellar granule cell growth and differentiation. J Neurosci Res *57*, 770-781.

Varadarajan, S.G., Kong, J.H., Phan, K.D., Kao, T.J., Panaitof, S.C., Cardin, J., Eltzschig, H., Kania, A., Novitch, B.G., and Butler, S.J. (2017). Netrin1 Produced by Neural Progenitors, Not Floor Plate Cells, Is Required for Axon Guidance in the Spinal Cord. Neuron *94*, 790-799 e793.

Wankhade, U.D., and Good, D.J. (2011). Melanocortin 4 receptor is a transcriptional target of nescient helix-loop-helix-2. Mol Cell Endocrinol *341*, 39-47.

Wilson, S.I., Shafer, B., Lee, K.J., and Dodd, J. (2008). A molecular program for contralateral trajectory: Rig-1 control by LIM homeodomain transcription factors. Neuron *59*, 413-424.

Wingate, R.J., and Hatten, M.E. (1999). The role of the rhombic lip in avian cerebellum development. Development *126*, 4395-4404.

Wu, Z., Makihara, S., Yam, P.T., Teo, S., Renier, N., Balekoglu, N., Moreno-Bravo, J.A., Olsen, O., Chédotal, A., Charron, F.*, et al.* (2019). Long-Range Guidance of Spinal Commissural Axons by Netrin1 and Sonic Hedgehog from Midline Floor Plate Cells. Neuron *101*, 635-647 e634.

Yamamoto, M., Boyer, A.M., Crandall, J.E., Edwards, M., and Tanaka, H. (1986). Distribution of stage-specific neurite-associated proteins in the developing murine

nervous system recognized by a monoclonal antibody. J Neurosci *6*, 3576-3594.

Yamauchi, K., Yamazaki, M., Abe, M., Sakimura, K., Lickert, H., Kawasaki, T., Murakami, F., and Hirata, T. (2017). Netrin-1 Derived from the Ventricular Zone, but not the Floor Plate, Directs Hindbrain Commissural Axons to the Ventral Midline. Sci Rep *7*, 11992.

Yee, K.T., Simon, H.H., Tessier-Lavigne, M., and O'Leary, D.M. (1999). Extension of long leading processes and neuronal migration in the mammalian brain directed by the chemoattractant netrin-1. Neuron *24*, 607-622.

Zelina, P., Blockus, H., Zagar, Y., Peres, A., Friocourt, F., Wu, Z., Rama, N., Fouquet, C., Hohenester, E., Tessier-Lavigne, M.*, et al.* (2014). Signaling switch of the axon guidance receptor Robo3 during vertebrate evolution. Neuron *84*, 1258-1272.

Zhu, Y., Hirata, T., Mackay, F., and Murakami, F. (2020). Chemokine receptor CXCR7 non-cell-autonomously controls pontine neuronal migration and nucleus formation. Sci Rep *10*, 11830.

Zhu, Y., Matsumoto, T., Nagasawa, T., Mackay, F., and Murakami, F. (2015). Chemokine Signaling Controls Integrity of Radial Glial Scaffold in Developing Spinal Cord and Consequential Proper Position of Boundary Cap Cells. J Neurosci *35*, 9211-9224.

FIGURE LEGENDS

Figure 1. In silico analyses of Nhlh1/2 binding sites on Robo3 promoter. (A) Predicted Nhlh1/2 binding sites across the 2 kb proximal promoter of mouse Robo3 by FIMO (MEME Suites) are indicated by blue color-filled boxes. The shades of blue indicate the range of p-values as shown by the legend. TSS: transcriptional start site. (B) Highly conserved regions in the 2 kb proximal promoters of Robo3 across six

divergent mammalian species were detected using mVISTA. The Y axes indicate percentage of identity. Pink and blue colored areas indicate regions with peak homology values above 70% upstream and downstream, respectively, of TSS. (C) Sequence alignment of the highly conserved regions indicated by the box with dashed line in (A) & (B) in the Robo3 promoters across six mammalian species. The red box in (C) highlights the sequences of the predicted Nhlh1/2 binding site.

Figure 2. Forced expression of full-length Nhlh1 and Nhlh2 induce ectopic Robo3 expression in the hindbrain and midbrain. (A) A schematic showing the experimental procedure. DNA constructs were introduced into the hindbrain or midbrain via in utero EP at E12.5, and the EP samples were analyzed at E14.5 on sections by Robo3 and GFP IHC. The approximate positions of sections shown for each region are indicated by red dashed lines. (B) A schematic showing a hindbrain section with EP unilaterally targeted to the dorsal hindbrain including the rhombic lip region (green). (C), (C') & (C'') A hindbrain section at low magnification with Robo3 and GFP IHC. EP and non-EP stand for electroporated and non-electroporated sides, respectively. The EP side, but not the non-EP side, showed induction of ectopic Robo3 expression (n = 6). (D), (D') & (D'') High magnification images of EP area (d) marked in (C''). The filled arrowheads indicate ectopic expression of Robo3 within the rhombic lip region. (E) A high magnification image of the non-EP area (e) marked in (C''). The hollow arrowheads indicate lack of Robo3 induction within the rhombic lip. (F), (F') & (F'') High magnification images of the EP area (f) in (C''). Many GFP positive neurons deep in the hindbrain epithelium also express ectopic Robo3. (G) A schematic showing a midbrain section with EP unilaterally targeted to the dorsal midbrain (green).

The boxed area shows the approximate region shown in (H) & (H'). (H) & (H') A midbrain section at low magnification with Robo3 and GFP IHC. The EP side, but not the non-EP side, showed induction of ectopic Robo3 expression (n = 3). (I), (I'), (I'') High magnification images of the EP area (i) marked in (H'). (J) A high magnification image of the non-EP area (j) marked in (H'). Scale bars: 200 μm in (C), (C') & (C''); 100 μm in (D), (D'), (D''), (E), (F), (F') & (F''); 200 μm in (H) & (H''); 100 μm in (I), (I'), (I'') & (J).

Figure 3. Nhlh1 and Nhlh2 are transcriptional activators in Robo3 induction and the arginine-rich domain upstream of bHLH domain is important for their inducibility. (A) Sequence alignment of Nhlh1 and Nhlh2 proteins shows a highly conserved C-terminal half encompassing a canonical bHLH domain and a stretch of 11 amino acids upstream of the bHLH with a consecutive run of arginine (R) (coined R6 domain in this study). The N-terminal halves of the two proteins are far less conservative and of low complexity structurally. (B) A schematic of constructs for testing Robo3 inducibility. VP16 is the potent transcriptional activation domain from the herpes simplex virus protein VP16. EnR is the potent transcriptional repressor domain from the drosophila protein Engrailed. (C), (D), (E), (F), (G) & (H) The rhombic lip regions of hindbrains electroporated with the indicated DNA constructs. Filled arrows indicate ectopic Robo3 induction in the rhombic lip in (D, n= 6), (E, n =3) and (H, n = 3), while hollow arrows indicate lack of Robo3 induction in (C, n = 5), (F, n = 3) and (G, n = 3). Scale bar: 100 μm in (C), (D), (E), (F), (G) & (H).

Figure 4. Forced expression of full-length Nhlh1 and Nhlh2 drive axonal projection towards the ventral midline. (A) A schematic showing the experimental procedure of testing the effect of force-expressing Nhlh1/2 on midbrain axonal trajectories. EP was performed at E11.5 into the dorsal midbrain, and the analysis of axonal trajectories of EP neurons was carried out on flat-mounted brainstems at E14.5. (B) Partial views of samples electroporated with either mCherry as control (n = 6), or with full-length Nhlh1/2 and mCherry constructs (n = 6). Fluorescence images were shown in the top panel, and those that merged with the brightfield images were shown in the bottom panel to visualize the positions of the ventral midline (indicated by vertical lines). (C) Quantification of the midbrain EP experiment. The commissural index is a measurement of the relative quantity of axons projecting to and reaching the ventral midline over those that projecting ipsilaterally (see materials and methods). Data were represented by a scatter plot, with the median and the upper and lower quantile indicated. Force-expressing Nhlh1 and Nhlh2 increased significantly the proportion of axons that crossed the ventral midline ($p = 0.0011$, Mann-Whitney U test). (D) The effect of expressing full-length Nhlh1/2 (n = 6) in comparison to expressing only EGFP construct (n = 7) on the trajectories of hindbrain axons. EP was performed at E12.5 into the dorsal hindbrain, and the analysis of axonal trajectories was carried out at E14.5 on sections of EP samples after GFP IHC. The vertical lines indicate the ventral midlines, and the bottom panel shows the high magnification images around the ventral midline regions corresponding to the boxed areas in the middle panel. (E) The quantification of the hindbrain EP experiment. The commissural index reflects the relative quantity of both axons and neurons reaching the vicinity of the ventral midline over those that are immediately below the rhombic lip (see materials and methods).

Data were represented by a scatter plot, with the median and the upper and lower quantile indicated. Force-expressing Nhlh1 and Nhlh2 increased significantly the proportion of axons and neurons that reached the ventral midline ($p = 0.0006$, Mann-Whitney U test). Scale bars: 400 μm in (B); 200 μm in (D).

Figure 5. Expression of Robo3, Nhlh1 and Nhlh2 on adjacent sections from the spinal cord to the midbrain by ISH. (A) The schematic on the left shows a hindbrain section at E14.5 with the cross-sections of migrating PN neurons in blue. The boxed area indicates region of the ISH images shown on the right. (B) & (C) Spinal cord sections at E11.5 and E13.5, respectively. (D) & (E) Caudal hindbrain sections at E11.5 and E13.5, respectively. (F) & (G) Rostral hindbrain sections at E11.5 and E13.5, respectively. (H) Midbrain sections at E11.5. Note the E13.5 midbrain data is not shown as Robo3 expression in the midbrain at this stage is very weak. Scale bars: 200 μm in (A); 200 μm in (B) & (C); 400 μm in (D) & (E); 400 μm in (F) & (G); 200 μm in (H).

Figure 6. PN neurons are positioned laterally without approaching the ventral midline in Nhlh1 and Nhlh2 double mutant. (A) A schematic showing the PN neuron migration and PN formation in an E16.5 hindbrain. Red dashed lines mark the rostrocaudal span of the sections shown in (B). (B) Sections across the PN region from an E16.5 hindbrain of the control genotype (top panel) and the double mutant (lower panel) with PN marked by Barhl1 IHC. PN neurons form a nucleus next to the ventral midline (arrows) ($n = 2$) in the control genotype, but were positioned in lateralized positions

(arrowheads) indicating failure to approach the ventral midline (n = 2). Scale bar: 200 μm in (B).

Figure 7. Lack of ventral commissures in the spinal cord, hindbrain and midbrain in Nhlh1 and Nhlh2 double mutant. Coronal sections from the spinal cord (A), caudal hindbrain (B), rostral hindbrain (C), and midbrain (D) at E11.5 were subjected to Tag1 and NF double IHC. The Tag1 signals label the commissural axons and the NF signals show the general axonal patterns. The DAPI counterstaining indicate the overall cytoarchitecture. Comparisons were made between the control genotype (*Nhlh1*$^{+/+}$ *Nhlh2*$^{+/m}$) (n = 3) and the double mutant (*Nhlh1*$^{m/m}$ *Nhlh2*$^{m/m}$) (n = 3). The Tag1 and NF merged images in the bottom panel are high magnification images of the ventral commissure regions. Filled arrows show the ventral commissures and the hollow arrows show the lack of ventral commissures. Scale bars: 200 μm in low magnification images in (A), (B), (C) & (D); 200 μm in high magnification images in (A), (B), (C) & (D).

Figure 8. Huge reduction of Robo3 expression in commissural neurons in Nhlh1 and Nhlh2 double mutant. Coronal sections from the spinal cord (A), caudal hindbrain (B), rostral hindbrain (C), and midbrain (D) at E11.5 were subjected to Robo3 and NF double IHC. A huge reduction of Robo3 expression was detected in the double mutant (n = 3) in comparison with the control genotype (n = 3) at these axial levels. (E) The schematics on the left show the migrating PN neurons in a whole mount E16.5 hindbrain in the top, and on a coronal section in the bottom. The red dashed line and the red boxed area indicate the approximate axial level and the area, respectively, of

IHC images on the right. PN neurons were labelled by Barhl1 IHC. A huge reduction of Robo3 expression in PN neurons was detected in the PN neurons in the double mutant (hollow arrow) (n = 2) in comparison with the control genotype (arrow) (n = 2). (F) & (G) Robo3 ISH on E11.5 spinal cord and E16.5 hindbrain sections, respectively, showed that Robo3 mRNA was markedly reduced in the double mutant. Scale bars: 100 μm in (A); 200 μm in (B); 400 μm in (C) & (D); 100 μm in (E); 100 μm in (F); 200 μm in (G).

Supplemental Figure 1. Expression of Nhlh1 and Nhlh2 in pre-crossing, and their down-regulation in post-crossing, PN neurons. (A) A schematic of a ventral view of an E15.5 hindbrain with the migratory stream of PN neurons indicated in blue. The red dashed lines indicate the approximate mediolateral positions of the three sets of sagittal sections shown in (a), (b) and (c). (B) A schematic of a ventral view of a hindbrain at E18.5 when most PN neurons have entered the nuclear region and become post-crossing. The red dashed line indicates the approximate position of the set of sagittal sections shown in (d). (a), (b), (c) & (d) ISH images selected from the Allen Developing Mouse Brain Atlas (https://developingmouse.brain-map.org/). PN neurons are marked by Barhl1 ISH (left panel), and Nhlh1 (mid panel) and Nhlh2 (right panel) ISH images were aligned with that of Barhl1 on sections of similar mediolateral levels. Arrows indicate the PN neurons. Scale bars: 800 μm in (a), (b) & (c); 800 μm in (d).

Supplemental Figure 2. Forced expression of either Nhlh1 or Nhlh2 alone induce moderate Robo3 expression. Full-length Nhlh1, or Nhlh2 was expressed together with nls-EGFP construct into the hindbrain or the midbrain at E12.5 and the samples were

analyzed for Robo3 induction by IHC at E14.5. (A), (A') & (A'') A hindbrain section EP with Nhlh1 and nls-EGFP constructs. A few cells in the rhombic lip expressed ectopic Robo3 (arrow) (n = 3). (B), (B') & (B'') A midbrain section EP with Nhlh1 and nls-EGFP constructs. A few cells in the midbrain expressed ectopic Robo3 (arrow) (n = 3). (C), (C') & (C'') A hindbrain section EP with Nhlh2 and nls-EGFP constructs. A few cells in the rhombic lip expressed ectopic Robo3 (arrow) (n = 2). (D), (D') & (D'') A midbrain section EP with Nhlh1 and nls-EGFP constructs. A few cells in the midbrain expressed ectopic Robo3 (arrow) (n = 2). Scale bar: 100 μm.

Supplemental Figure 3. Forced expression of full-length Lhx2 does not induce ectopic Robo3 expression in the hindbrain and the midbrain. (A) and (E) Schematics showing a hindbrain section and a midbrain section with EP targeting mainly to the rhombic lip region (green), and the left dorsal midbrain (green), respectively. Samples were subjected to Robo3 and GFP IHC. (B), (C) & (D) A region of a hindbrain section corresponding to the red boxed region in (A). Robo3 was not induced within the rhombic lip region as indicated by the hollow arrows (n = 3). (F), (G) & (H) A region of a midbrain section corresponding to the red boxed region in (E). Robo3 was not induced in the midbrain by Lhx2 EP (n = 2). Scale bar: 100 μm in (B), (C), (D), (F), (G) & (H).

Supplemental Figure 4. Forced expression of Nhlh1 and Nhlh2 induce Robo3 transcription. Full-length Nhlh1 and Nhlh2 were electroporated together with nls-EGFP into the hindbrain or the midbrain at E12.5 and the samples were analyzed for Robo3 induction by ISH at E14.5. (A) & (A'') The EP and non-EP side of an

electroporated hindbrain. The EP side only showed induction of Robo3 mRNA within the rhombic lip. (B) A section of an electroporated midbrain. The EP side only showed induction of Robo3 mRNA. Scale bar: 200 μm.

Supplemental Figure 5. Robo3 inducibility of VP16- and EnR-fusion constructs in the midbrain. VP16 fused full-length or truncated Nhlh1/2, or EnR fused full-length Nhlh1/2 (see Figure 3B) were electroporated into the midbrain at E12.5 and samples were analyzed at E14.5 by Robo3 IHC. (A) Nhlh1/2-fl-VP16 (n = 2) and (D) R6-bHLH1/2-VP16 (n = 2) induced Robo3 expression, but (B) Nhlh1/2-fl-EnR (n = 2) and (C) bHLH1/2-VP16 (n = 2) failed to induce Robo3. Scale bar: 100 μm.

Supplemental Figure 6. Robo3 expression is not well correlated with that of Nhlh1 and Nhlh2 in brain structures rostral to the midbrain. (A) Robo3 is expressed in GE at E11.5, but not Nhlh1 and Nhlh2. (B) Robo3-positive neurons in HTH at E13.5 do not appear to express Nhlh1 and Nhlh2. (C) mHb neurons in the E13.5 epithalamus express Robo3, but they either do not or only partially express Nhlh1 and Nhlh2. GE: ganglionic eminence; HTH: hypothalamus; mHb: medial habenular nucleus. Scale bar: 200 μm.

Supplemental Figure 7. Generation of Nhlh1 and Nhlh2 mutant alleles by CRISPR-Cas9 gene editing in fertilized eggs. (A) Sequences of the two sgRNAs used for Nhlh1 and Nhlh2 alleles, respectively. (B) A schematic showing the approximate positions of the two sgRNAs on the Nhlh1, or Nhlh2 locus. (C) & (D) Alignment of DNA sequences and protein sequences between the wild type and Nhlh1 mutant allele, and

between the wild type and Nhlh2 mutant allele, respectively. (E) EP of constructs expressing Nhlh1 and Nhlh2 mutant proteins in the hindbrain did not induce ectopic Robo3 expression within the rhombic lip (n = 2). (F) EP of constructs expressing Nhlh1 and Nhlh2 mutant proteins in the migrating PN neurons did not suppress their Robo3 expression (n = 2). Scale bars: 100 μm in (E); 100 μm in (F).

Supplemental Figure 8. PN formation is normal in Nhlh1 and Nhlh2 single mutant. PN neurons were labelled by Barhl1 IHC on E16.5 rostral hindbrain sections. PN position, shape and size were comparable between the heterozygotes and homozygotes of Nhlh1 mutant (A) (n = 3) and Nhlh2 mutant (B) (n = 2). Scale bar: 200 μm.

Supplemental Figure 9. IO nucleus is lateralized in Nhlh1 and Nhlh2 double mutant. IO neurons were labelled by FoxP2 IHC at E13.5 (A) and E16.5 (B). IO neurons appeared lateralized and stayed at a distance away from the ventral midbrain in the double mutant (arrows, n = 2 for E13.5, and n = 2 for E16.5), whereas in the control genotype, they were in close juxtaposition to the ventral midline (arrows, n = 2 for E13.5, and n = 2 for E16.5). Scale bar: 200 μm.

Supplemental Figure 10. Commissure formation does not appear to be affected in Nhlh1 and Nhlh2 single mutant. Commissural axons were labelled by Tag1 IHC, and the overall axonal patterns were labelled by NF IHC. Ventral commissure appears comparable between the control genotype of $Nhlh1^{+/+}Nhlh2^{+/m}$ (n = 2), and the mutant genotypes of $Nhlh1^{+/m}Nhlh2^{m/m}$ (n = 2) and $Nhlh1^{m/m}Nhlh2^{+/m}$ (n = 2), in the spinal cord (A), caudal hindbrain (B), rostral hindbrain (C), and midbrain (D). Higher

magnification images of the commissural region across the ventral midline are shown in the bottom panels. Scale bars: 100μm in (A); 200 μm in (B), (C) & (D).

Supplemental Figure 11. Commissure-less phenotype in the Nhlh1 and Nhlh2 double mutant persisted into later developmental stages. Commissure formation was analyzed either by Tag1 or NF IHC. Lack of commissure formation continued to be observed in E13.5 spinal cord (A) (n = 2 for each genotype), E16.5 spinal cord (B) (n = 2 for each genotype), E13.5 hindbrain (C) (n = 2 for each genotype) and E13.5 midbrain (D) (n = 2 for each genotype). Scale bars: 200 μm in (A); 100 μm in (B); 400 μm in (C) & (D).

Supplemental Figure 12. Commissure formation not via FP is unaffected in Nhlh1 and Nhlh2 double mutant. Commissural axons crossing the midline dorsally in the spinal cord, labelled by L1CAM IHC was comparable between the control and the double mutant (A) (n = 2 for each genotype). Commissure formation in structures rostral to the midbrain, such as the anterior commissure (B) and the corpus callosum (C), both labelled by L1CAM, appear comparable between the control and the double mutant (n = 2 for each genotype). Scale bars: 200 μm in (A); 500 μm in (B) & (C).

Supplemental Figure 13. Extrinsic guidance molecules known to guide commissural axons towards the FP, Netrin-1 and Shh, are not altered in the Nhlh1 and Nhlh2 double mutant. Netrin-1 and Shh expression were examined by ISH. Netrin-1 (A) and Shh (B) distribution were comparable between the control and the double mutant. Scale bars: 200 μm in (A); 200 μm in (B).

Supplemental Figure 14. Generation of commissural neurons and their expression of guidance receptor DCC are unaffected in the Nhlh1 and Nhlh2 double mutant. (A) DCC expression pattern was similar between the control and the double mutant in the dorsal half of the spinal cord where most spinal commissural neurons reside (n = 3 for each genotype). (B) Spinal cord sections of control and double mutant were subjected to Brn3a IHC. Brn3a expressing spinal neurons which encompassing several classes of both ipsi-lateral and commissural dorsal spinal neurons were similar in numbers between the control (n = 3) and the double mutant (n = 3) as shown by the quantification depicted in the scatter plot. (C) DCC IHC on E16.5 hindbrain sections show that DCC is expressed at a similar level between the control (n = 2) and the double mutant (n = 2). Scale bars: 100 μm in (A); 100 μm in (B); 200 μm in (C).

Supplemental Figure 15. Robo3 expression is not affected in brain structures rostral to the midbrain in the Nhlh1 and Nhlh2 double mutant. Robo3 expression was examined by IHC. Robo3 expression level is comparable between the control and the double mutant, in the GE at E11.5 (A) (n = 2 for each genotype), in the mHB at E13.5 (B) (n = 2 for each genotype), in the HTH at E13.5 (C) (n=2 for each genotype), in the caudally extending FR at E13.5 (D) (n = 2 for each genotype), and in the FR crossing the ventral midline at the midbrain/hindbrain junction at E13.5 (E) (n = 2 for each genotype). GE: Ganglionic Eminence; mHb: medial habenular nucleus; HTH: hypothalamus; FR: fasciculus retroflexus. Scale bar: 400 μm.

Supplemental Figure 16. Dbx1 forced expression in the midbrain at E11.5 induces ectopic expression of Nhlh2 concomitantly with Robo3. An expression plasmid co-

expressing Dbx1 and nls-EGFP was electroporated into E11.5 midbrains and samples were analyzed at E14.5 (n=2). (A) Ectopic expression of Robo3 (arrow in the bottom panel) was induced by Dbx1 (GFP positive area), in line with a previously study (Inamata and Shirasaki, 2014). (B) ISH with a Nhlh2 probe on a section adjacent to the section in (A). Nhlh2 ISH signal is clearly increased at the EP site (arrow) compared with the equivalent region at the non-EP side. (C) Higher magnification mages of the boxed regions in (B). We also performed ISH with the Nhlh1 probe, however, Nhlh1 ISH at E14.5 appeared somewhat diffused, hampering clear comparison between the EP and non-EP sides. Scale bars: 200 μm in (A); 200 μm in (B); 200 μm in (C).

Figure 1

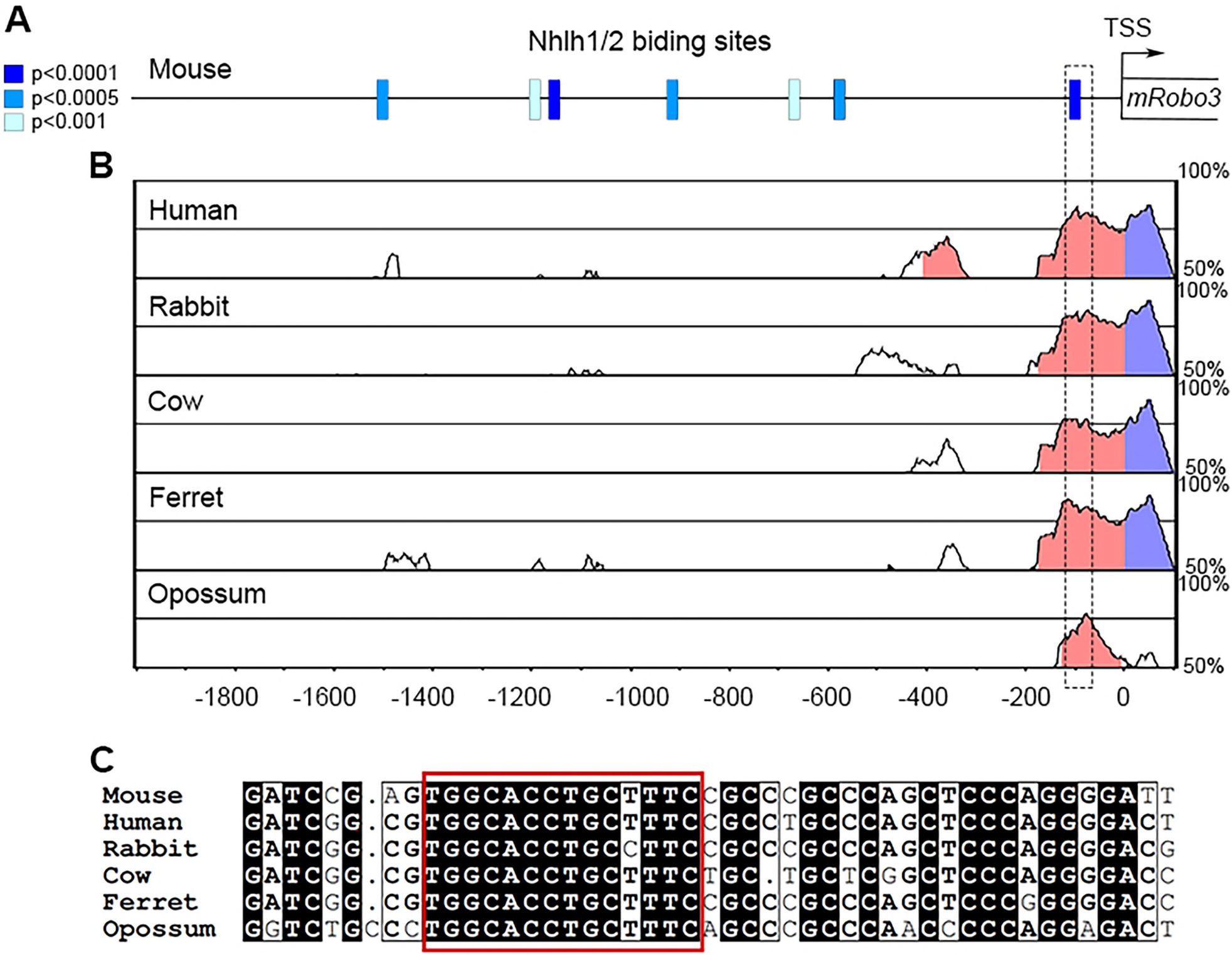
A
p<0.0001
p<0.0005
p<0.001
Mouse
Nhlh1/2 biding sites
TSS
mRobo3
B
Human
Rabbit
Cow
Ferret
Opossum
100%
50%
-1800
-1600
-1400
-1200
-1000
-800
-600
-400
-200
0
C
Mouse GATCCG.AGTGGCACCTGCTTTCCGCCCGCCCAGCTCCCAGGGGATT
Human GATCGG.CGTGGCACCTGCTTTCCGCCTGCCCAGCTCCCAGGGGACT
Rabbit GATCGG.CGTGGCACCTGCCTTCCGCCCGCCCAGCTCCCAGGGGACG
Cow GATCGG.CGTGGCACCTGCTTTCTGC.TGCTCGGCTCCCAGGGGACC
Ferret GATCGG.CGTGGCACCTGCTTTCCGCCCGCCCAGCTCCCGGGGGACC
Opossum GGTCTGCCCTGGCACCTGCTTTCAGCCCGCCCAACCCCCAGGAGACT

Figure 2

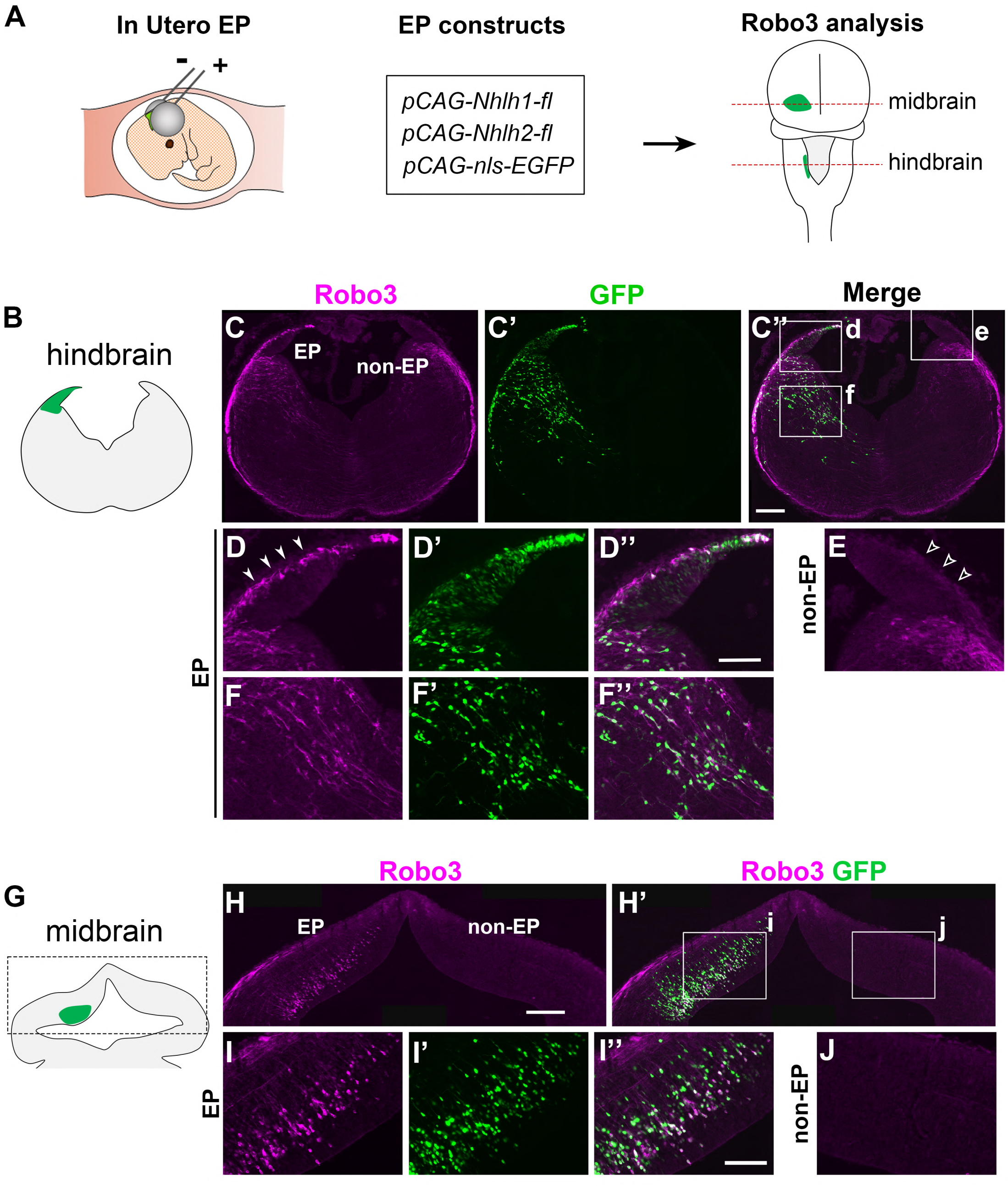
A
In Utero EP
-
+
EP constructs
pCAG-Nhlh1-fl
pCAG-Nhlh2-fl
pCAG-nls-EGFP
Robo3 analysis
midbrain
hindbrain
B
hindbrain
Robo3
GFP
Merge
C
EP
non-EP
C'
C''
d
e
f
D
D'
D''
E
F
F'
F''
EP
non-EP
G
midbrain
Robo3
Robo3 GFP
H
EP
non-EP
H'
i
j
I
I'
I''
J
EP
non-EP

Figure 3

A

```
Nhlh1   MMLNSDTME-LDLPPT-HSETES----------GFSDCGGGPGPDGAGSGDPGVVQVRSS   48
Nhlh2   MMLSPDQAADSDHPSSTHSDPESLGGADTKVLGSVSDLEPVEEADGDGKGGSR-------   53
        ***. *     * * : **: **          ..**       ** *.*.
                    R6          basic          Helix I
Nhlh1   ELGESGRKDLQHLSREERRRRRRATAKYRTAHATRERIRVEAFNLAFAELRKLLPTLPPD   108
Nhlh2   ---AALYPHPQQLSREEKRRRRRATAKYRSAHATRERIRVEAFNLAFAELRKLLPTLPPD   110
            :    . *:*****:***********:*****************************
                 Helix II
Nhlh1   KKLSKIEILRLAICYISYLNHVLDV   133
Nhlh2   KKLSKIEILRLAICYISYLNHVLDV   135
        ************************
```

B

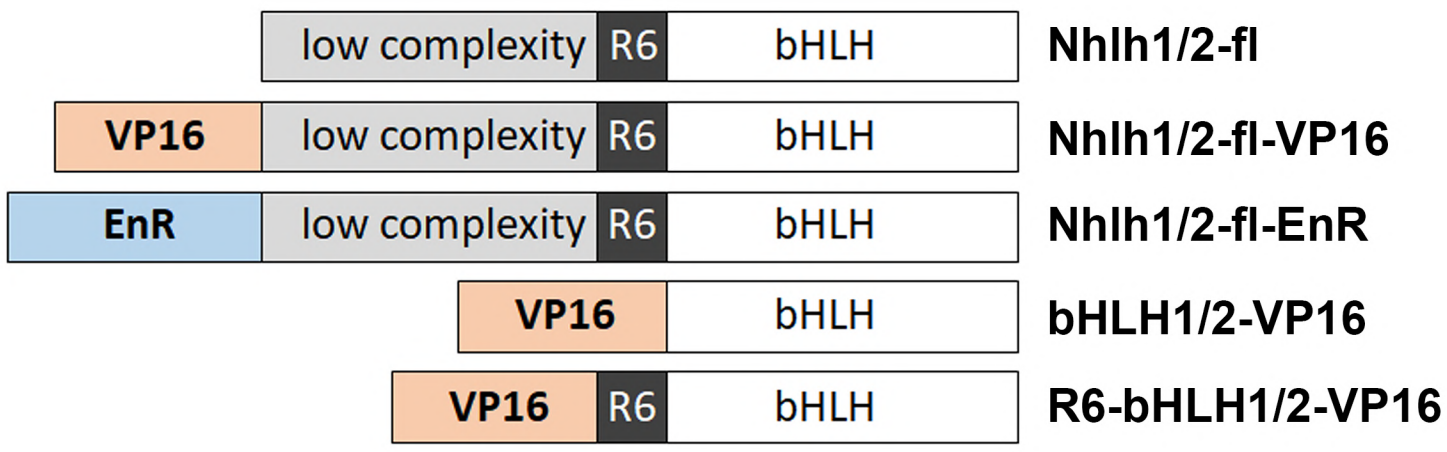

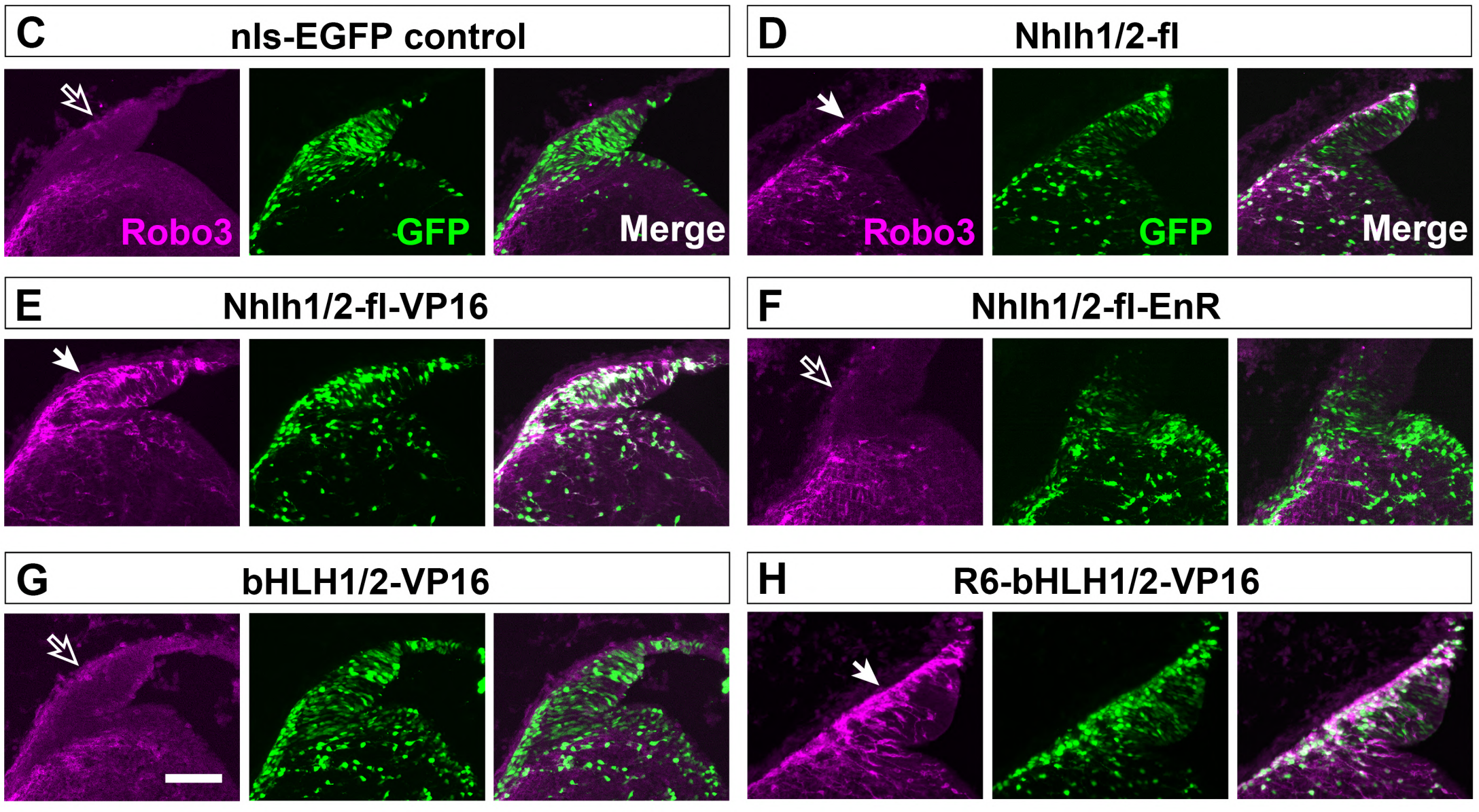

Figure 4

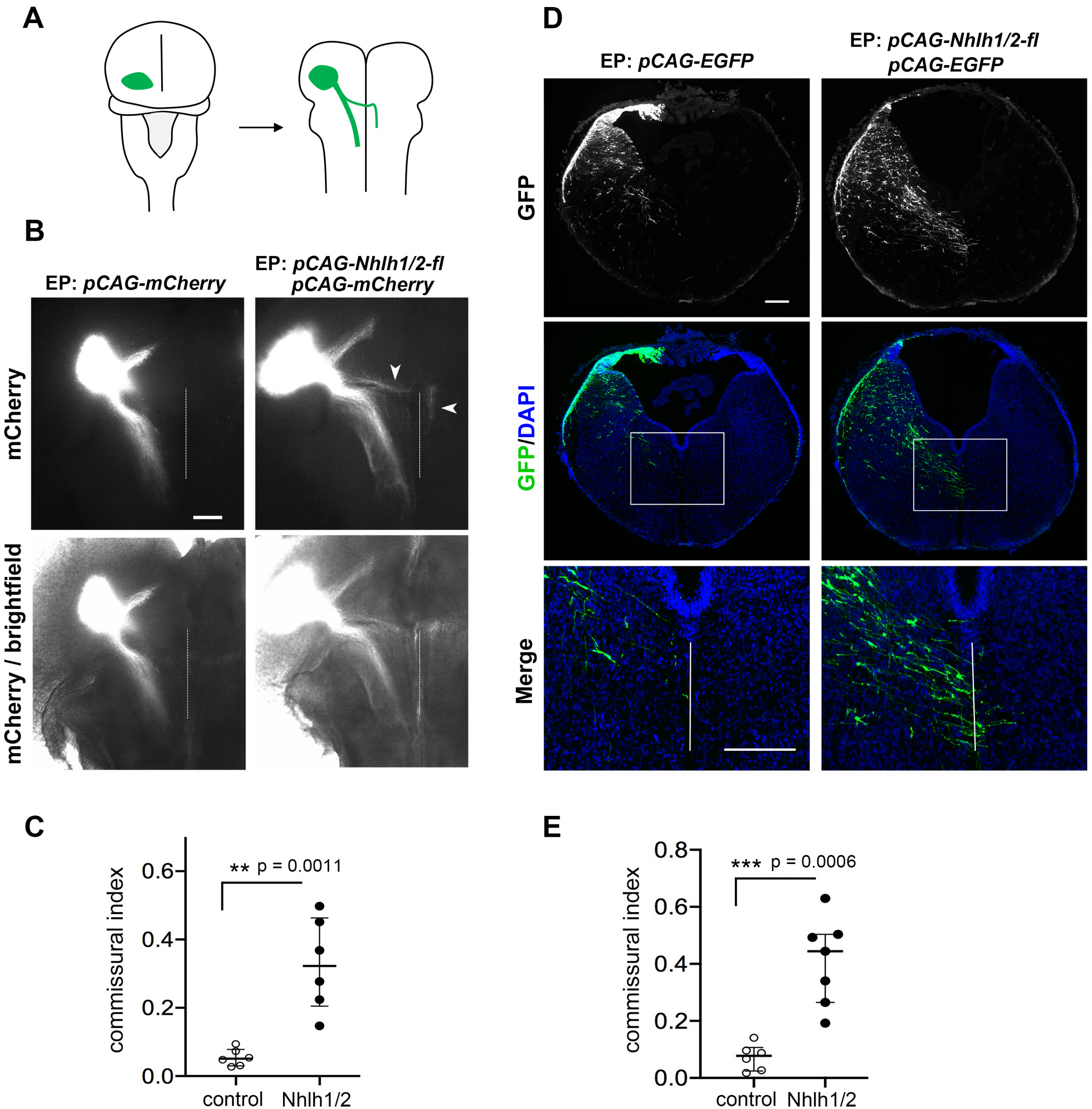
A
B
EP: pCAG-mCherry
EP: pCAG-Nhlh1/2-fl
pCAG-mCherry
mCherry
mCherry / brightfield
D
EP: pCAG-EGFP
EP: pCAG-Nhlh1/2-fl
pCAG-EGFP
GFP
GFP/DAPI
Merge
C
commissural index
** p = 0.0011
0.0
0.2
0.4
0.6
control
Nhlh1/2
E
commissural index
*** p = 0.0006
0.0
0.2
0.4
0.6
0.8
control
Nhlh1/2

Figure 5

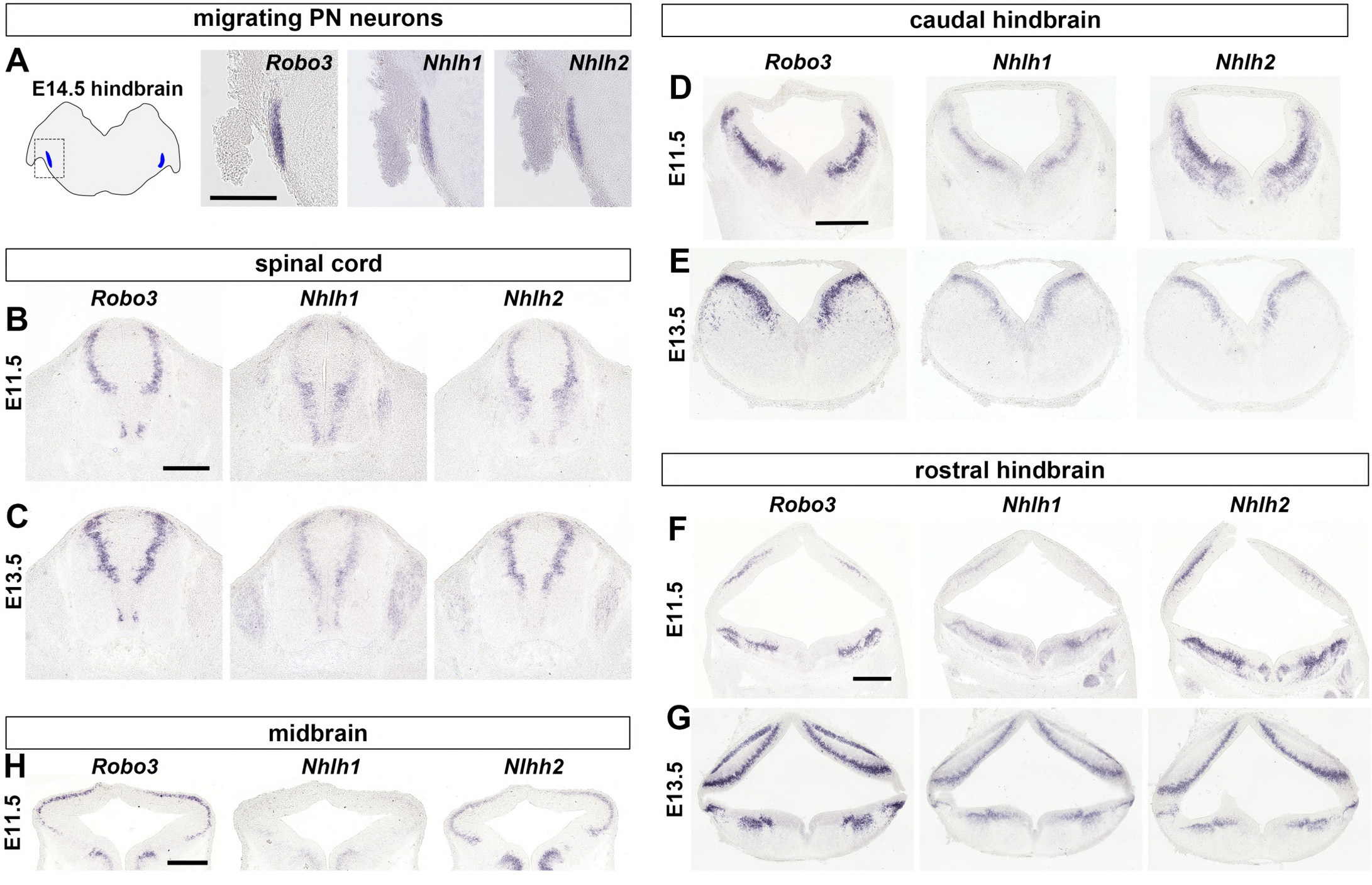
migrating PN neurons
A
E14.5 hindbrain
Robo3
Nhlh1
Nhlh2
spinal cord
B
E11.5
Robo3
Nhlh1
Nhlh2
C
E13.5
midbrain
H
E11.5
Robo3
Nhlh1
Nlhh2
caudal hindbrain
D
E11.5
Robo3
Nhlh1
Nhlh2
E
E13.5
rostral hindbrain
F
E11.5
Robo3
Nhlh1
Nhlh2
G
E13.5

Figure 6

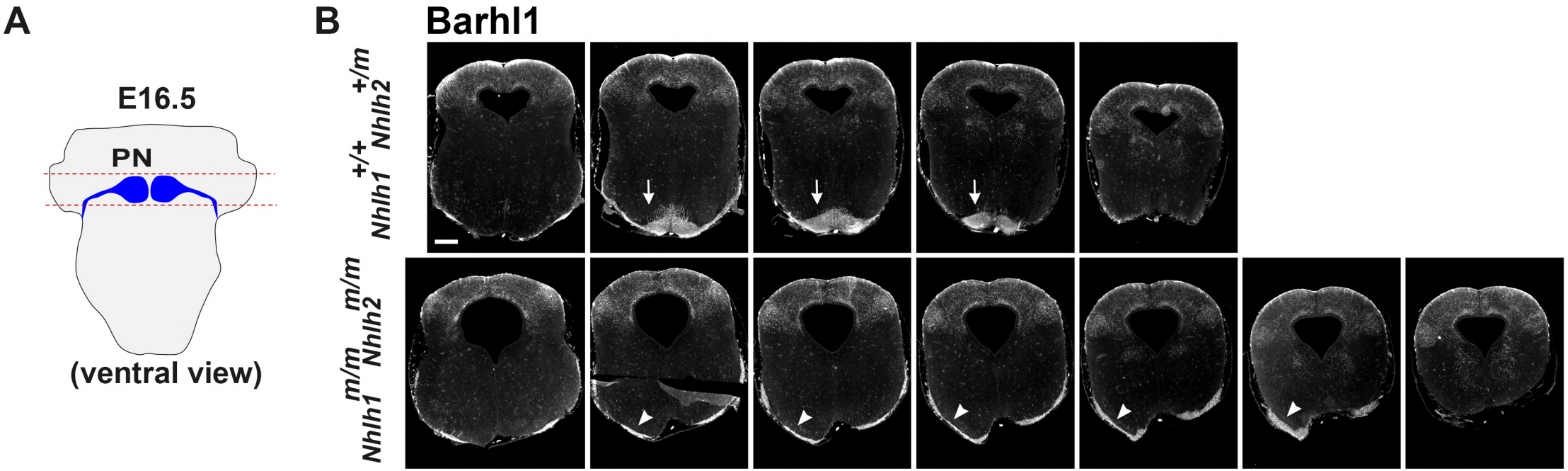
A
E16.5
PN
(ventral view)
B
Barhl1
+/+ Nhlh1
+/m Nhlh2
m/m Nhlh1
m/m Nhlh2

Figure 7

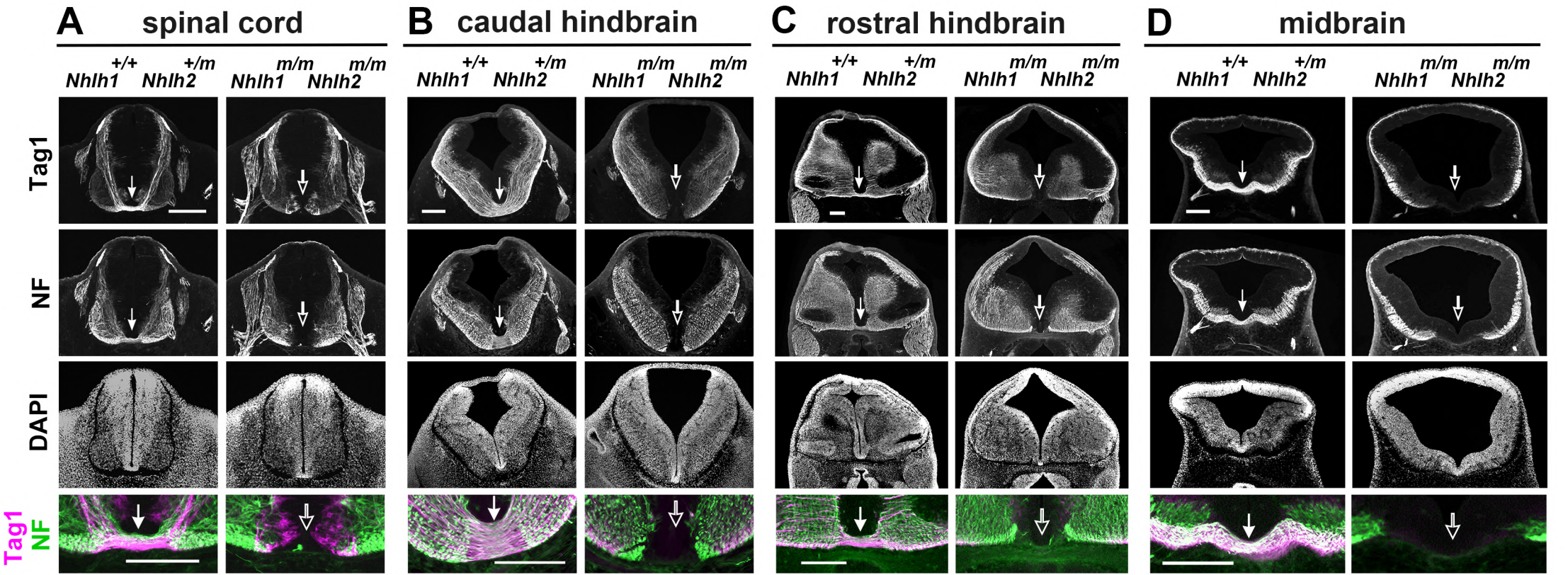
A spinal cord
B caudal hindbrain
C rostral hindbrain
D midbrain
Nhlh1 +/+ Nhlh2 +/m
Nhlh1 m/m Nhlh2 m/m
Tag1
NF
DAPI
Tag1
NF

Figure 8

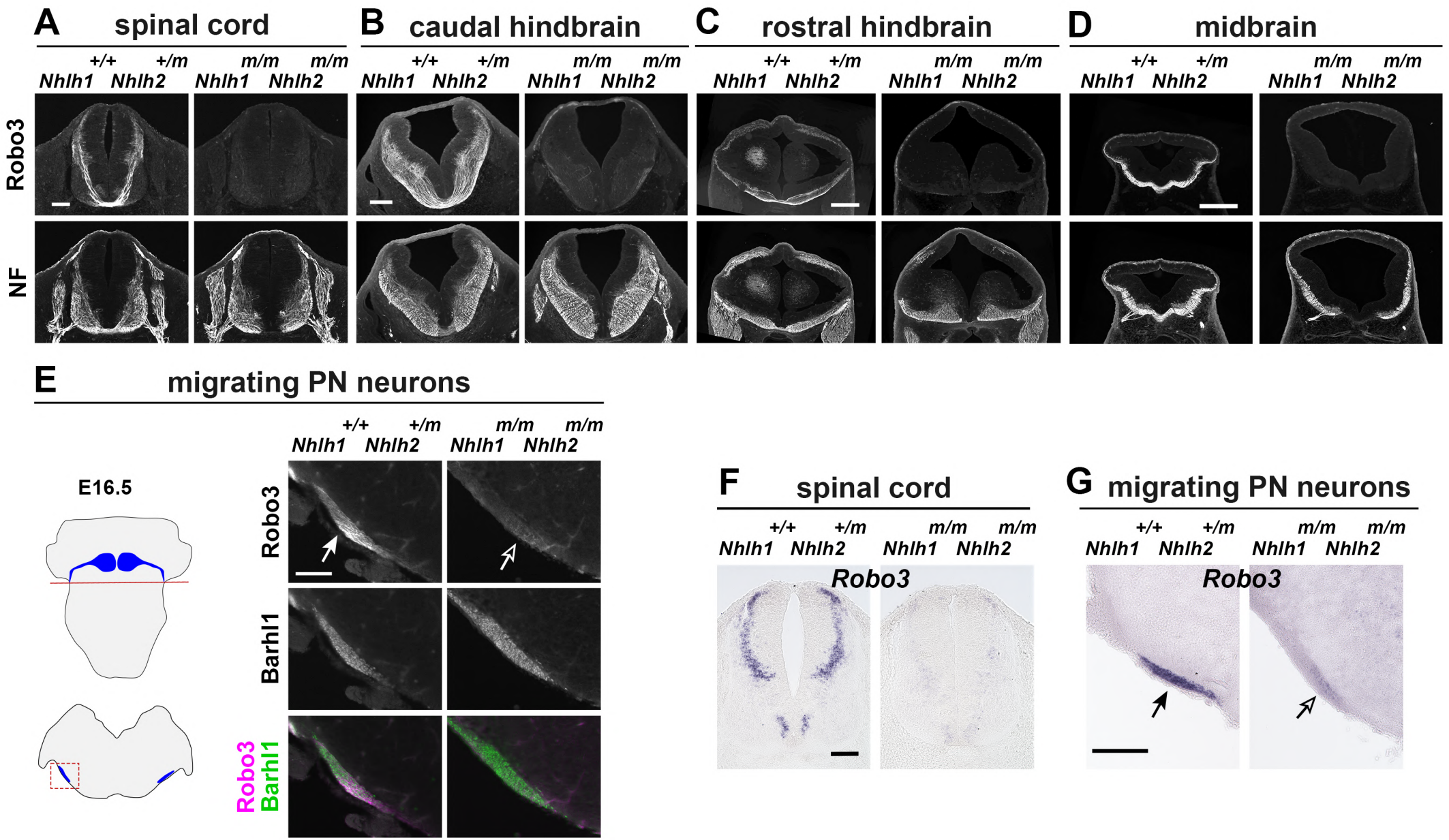
A spinal cord
B caudal hindbrain
C rostral hindbrain
D midbrain
+/+ +/m m/m m/m
Nhlh1 Nhlh2 Nhlh1 Nhlh2
Robo3
NF
E migrating PN neurons
E16.5
Robo3
Barhl1
Robo3
Barhl1
F spinal cord
Robo3
G migrating PN neurons
Robo3

Supplemental Figure 1

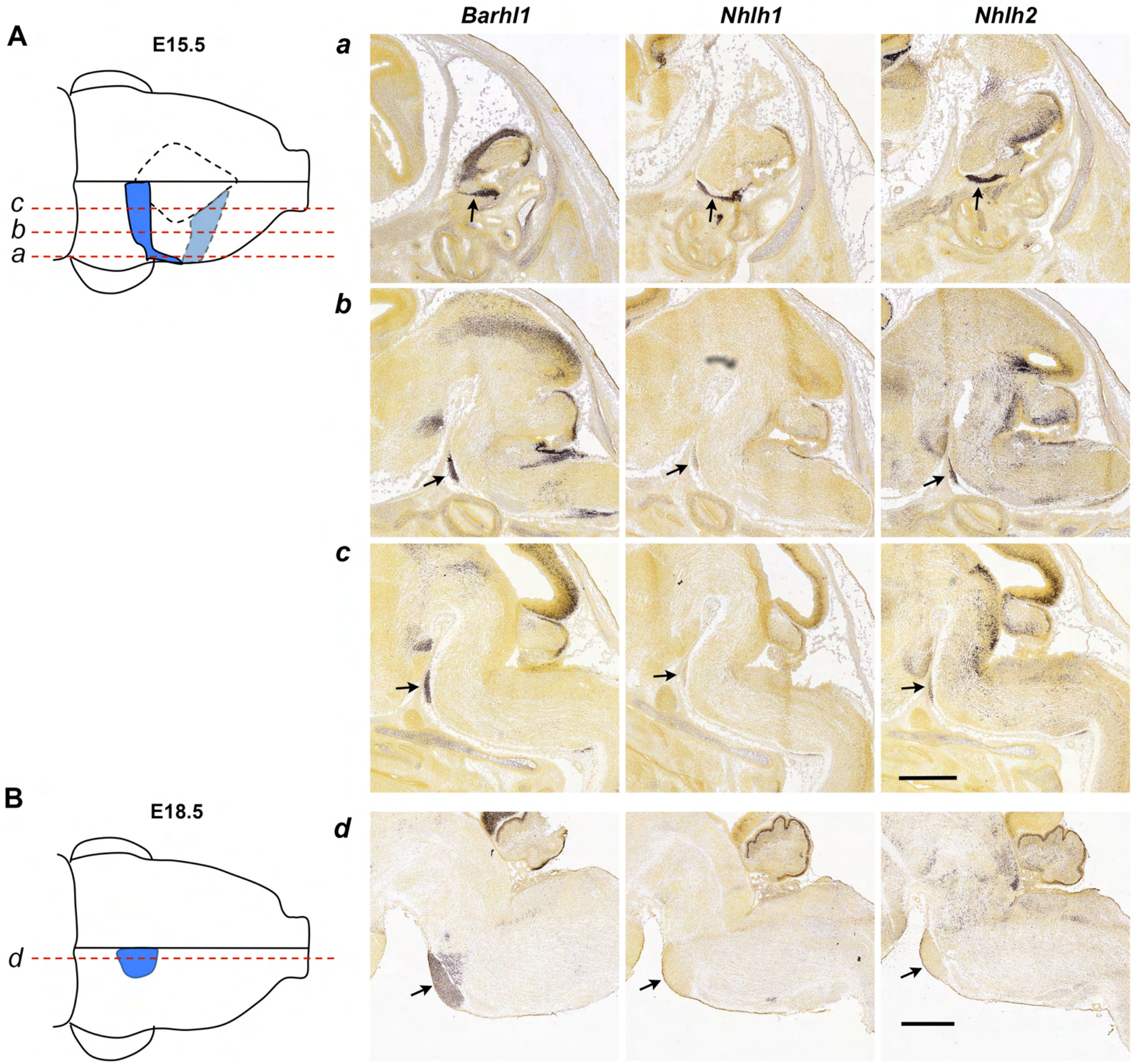

Supplemental Figure 2

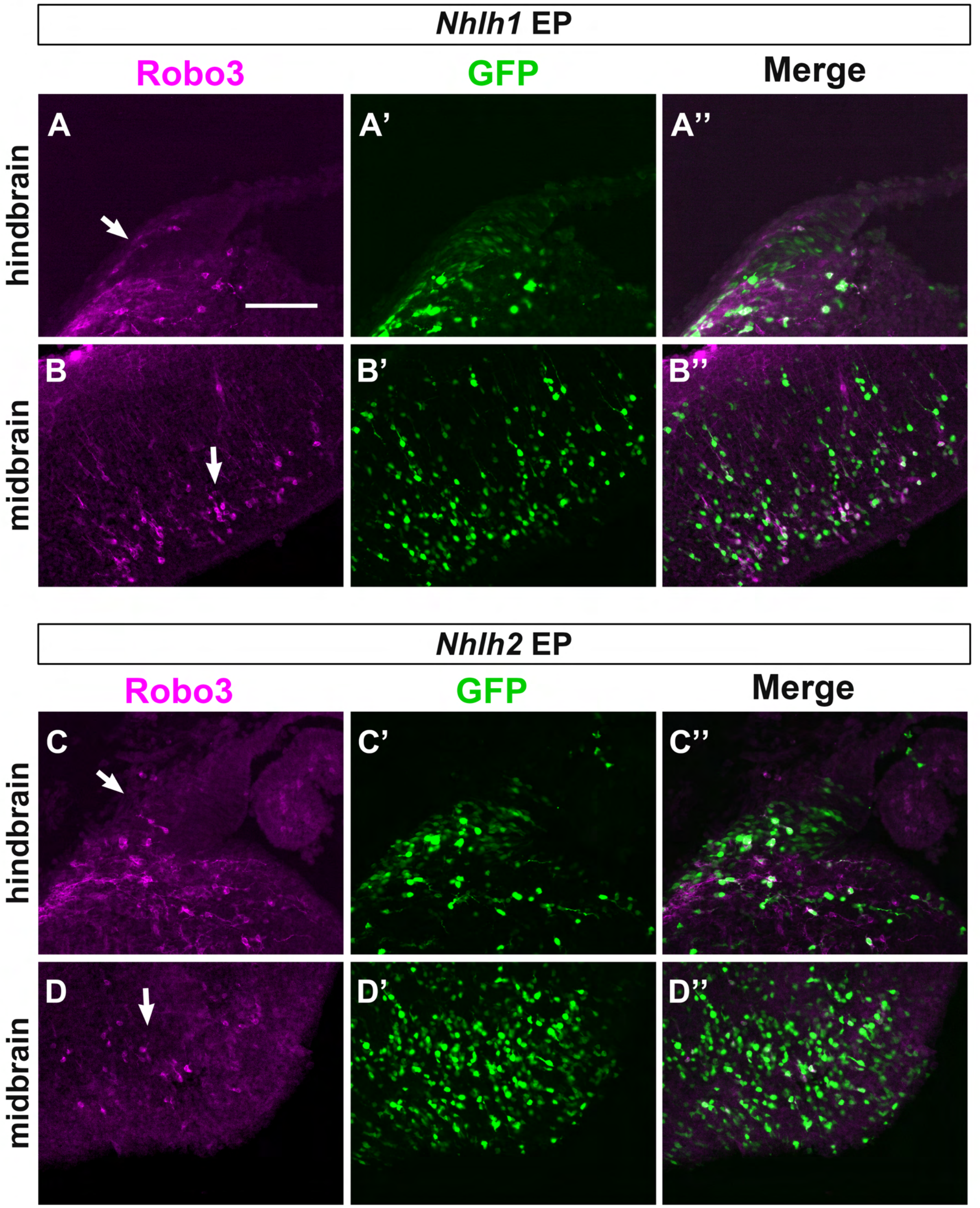

Supplemental Figure 3

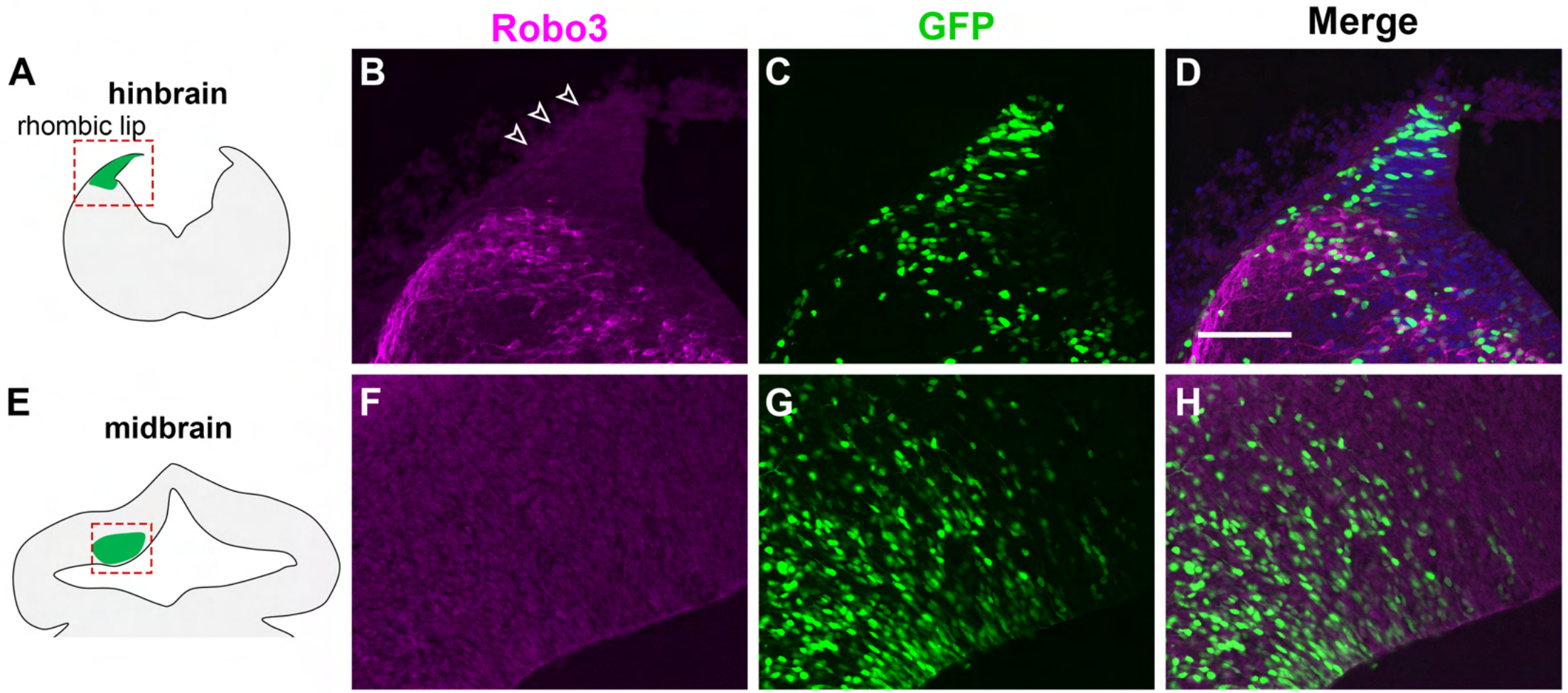

Supplemental Figure 4

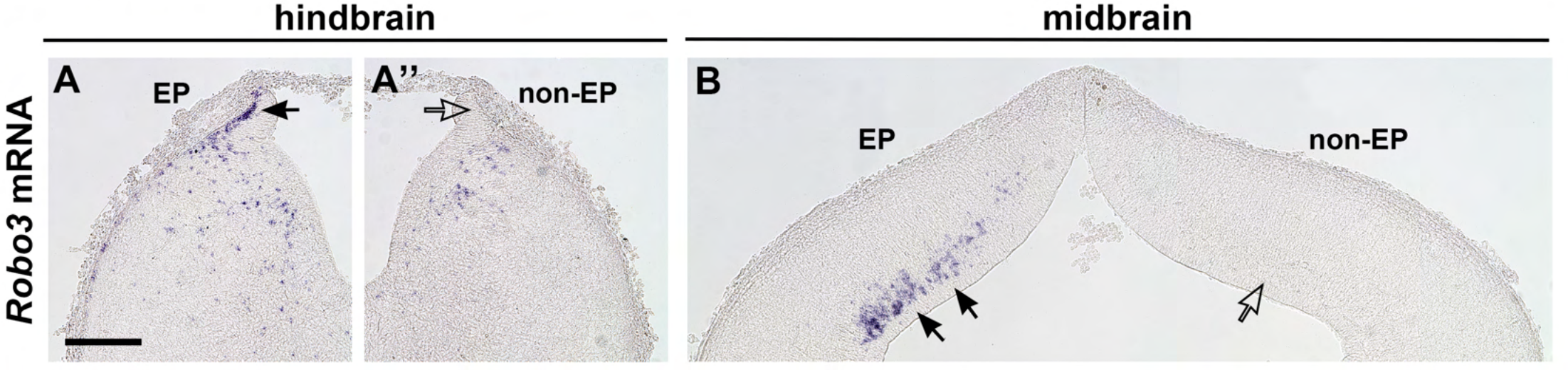

Supplemental Figure 5

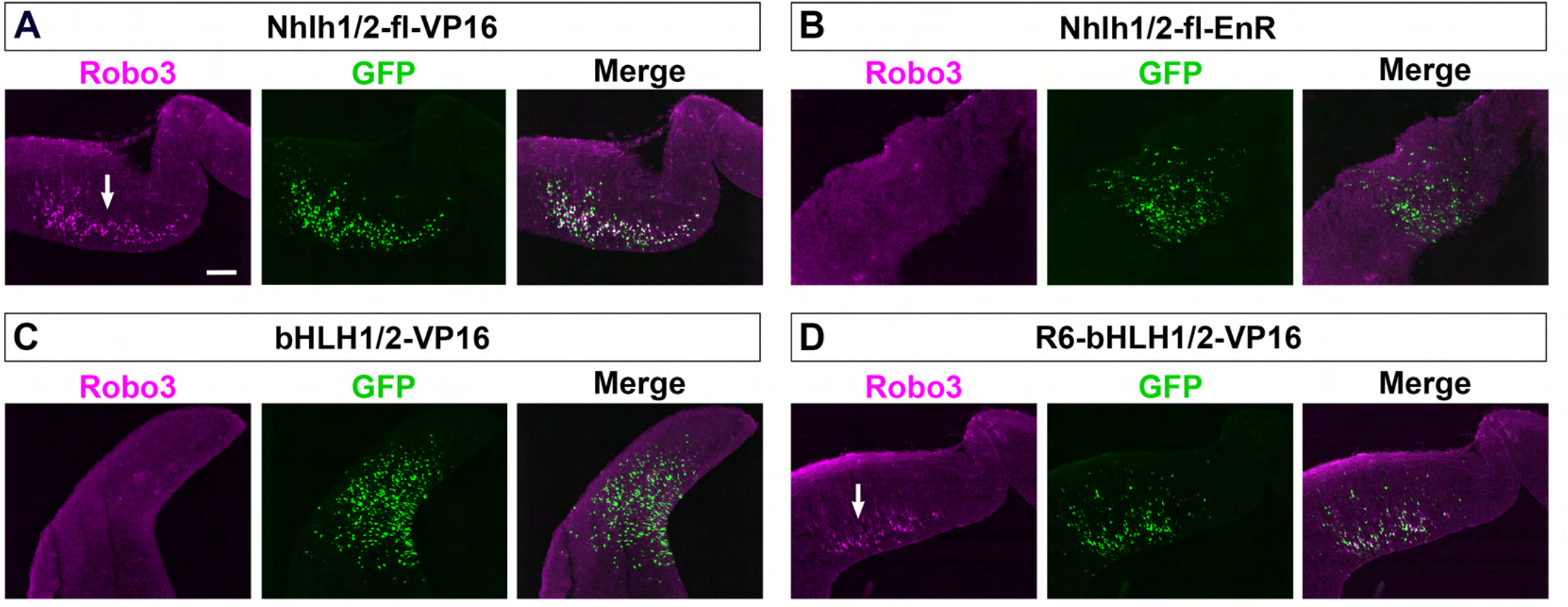

Supplemental Figure 6

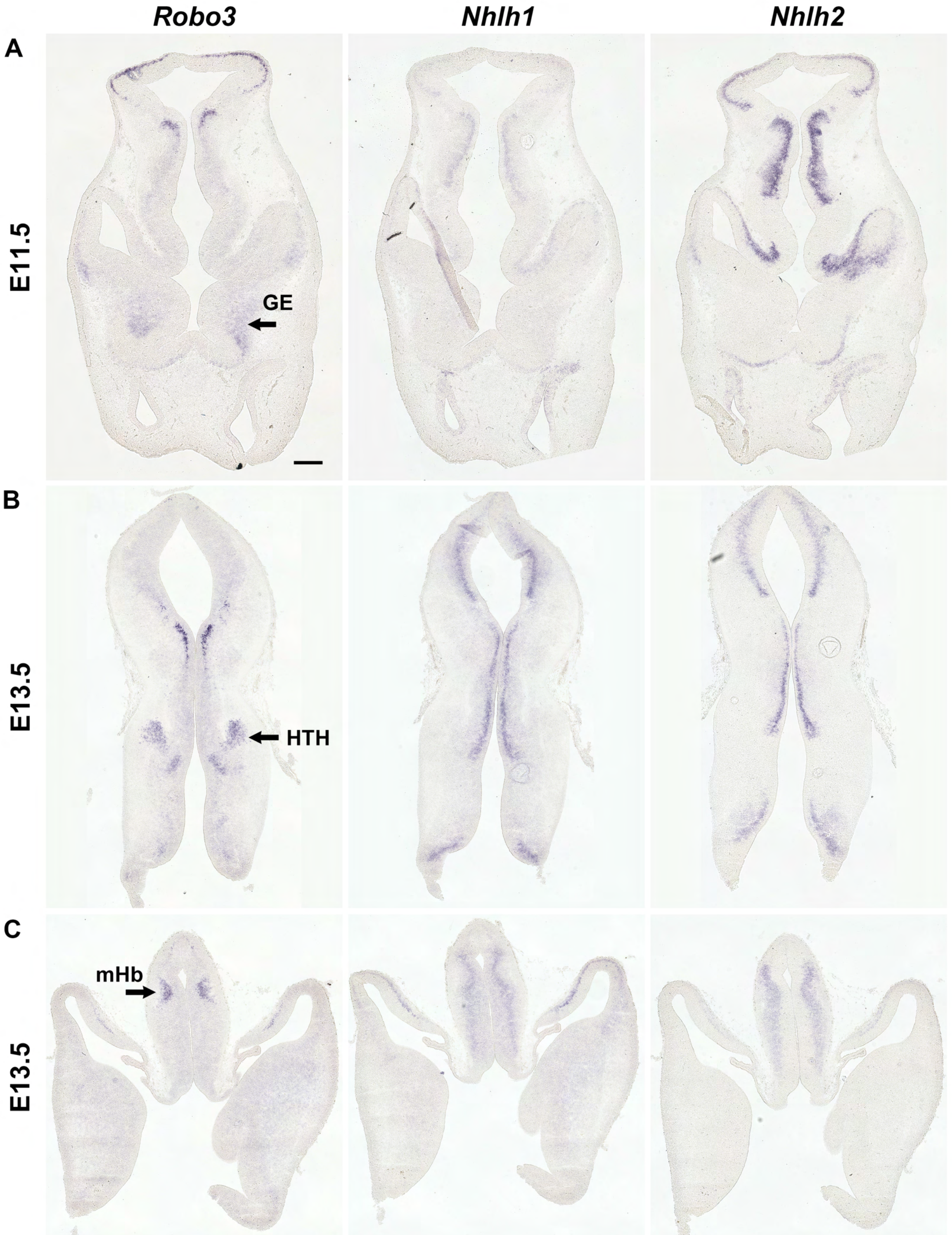

Supplemental Figure 7

A

		sgRNA sequence
Nhlh1	sgRNA1	GGACCGGGCCCCGATGGTGC
	sgRNA2	GCTAGGTTGAAGGCTTCCACG
Nhlh2	sgRNA1	GCGAAGAAAAGCGCCGCCGC
	sgRNA2	GTTCTTGTCCGGAGGCAGCGT

B

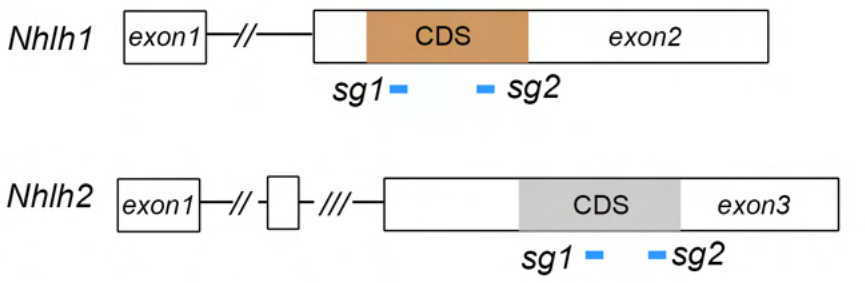

C

alignment of Nhlh1 DNA seq

```
    WT TCGGGCTTTAGCGACTGTGGGGGCGGACCGGGCCCCGATGGTGCTGGATCCGGGGATCCA   120
Nhlh1-m TCGGGCTTTAGCGACTGTGGGGGCGGACCGGGCCCCGAT--------------GATCCA   105
        ************************************              ******

    WT GGAGTGGTCCAGGTCCGGAGCTCAGAGCTTGGAGAGTCCGGCCGCAAAGACCTGCAGCAC   180
Nhlh1-m GGAGTGGTCCAGGTCCGGAGCTCAGAGCTTGGAGAGTCCGGCCGCAAAGACCTGCAGCAC   165
        ************************************************************

    WT TTGAGTCGTGAGGAGCGCAGGCGCCGGCGCCGCGCCACGGCCAAGTACCGCACGGCACAC   240
Nhlh1-m TTGAGTCGTGAGGAGCGCAGGCGCCGGCGCCGCGCCACGGCCAAGTACCGCACGGCACAC   225
        ************************************************************

    WT GCCACGCGGGAGCGCATCCGCGTGGAAGCCTTCAACCTAGCCTTCGCCGAGCTGCGCAAG   300
Nhlh1-m GCCA--------------------CGCCTTCAACCTAGCCTTCGCCGAGCTGCGCAAG   263
        ****                     ******************************
```

alignment of Nhlh1 protein seq

```
    WT MMLNSDTMELDLPPTHSETESGFSDCGGGPGPDGAGSGDPGVVQVRSSELGESGRKDLQH
Nhlh1-m MMLNSDTMELDLPPTHSETESGFSDCGGGPGPD-----DPGVVQVRSSELGESGRKDLQH
        ********************************     *********************

                                   helix
    WT LSREERRRRRRATAKYRTAHATRERIRVEAFNLAFAELRKLLPTLPPDKKLS-----KIE
Nhlh1-m LSREERRRRRRATAKYRTAHATPST*PSPSCASCC----PLCPRTRSSLRLRSYAWPSAI
        ********************* .     :   .      * *    . :*      .
        helix
    WT ILRLAICYISYLNHVLDV   133
Nhlh1-m SPT*TMCWTS--------   119
           ::*: *
```

D

alignment of Nhlh2 DNA seq

```
    WT GTGGAGGAGGCGGACGGCGACGGCAAGGGAGGCAGCCGGGCCGCGCTCTACCCGCACCCG   180
Nhlh2-m GTGGAGGAGGCGGACGGCGACGGCAAGGGCGGCAGCCGGGCCGCGCTCTACCCGCACCCG   180
        **************************** ****************************

    WT CAGCAGCTGAGCCGCGAAGAAAAGCGCCGC-CGCCGGCGCGCCACGGCCAAGTACCGATC   239
Nhlh2-m CAGCAGCTGAGCCGCGAAGAAAAGCGCCGCGCGCCGGCGCGCCACGGCCAAGTACCGATC   240
        **************************** ****************************

    WT GGCCCACGCCACCCGCGAGCGCATCCGAGTGGAGGCTTTCAACCTGGCCTTCGCCGAGCT   299
Nhlh2-m GGCCCACGCCACCCGCGAGCGCATCCGAGTGGAGGCTTTCAACCTGGCCTTCGCCGAGCT   300
        ************************************************************

    WT CCGCAAACTACTACCCACGCTGCCTCCGGACAAGAAGCTCTCCAAGATCGAGATTCTGCG   359
Nhlh2-m CCGCAAACTACTAC---------TCCGGACAAGAAGCTCTCCAAGATCGAGATTCTGCG   350
        **************         ***********************************
```

alignment of Nhlh2 protein seq

```
    WT MMLSPDQAADSDHPSSTHSDPESLGGADTKVLGSVSDLEPVEEADGDGKGGSRAALYPHP
Nhlh2-m MMLSPDQAADSDHPSSTHSDPESLGGADTKVLGSVSDLEPVEEADGDGKGGSRAALYPHP
        ************************************************************

                                   helix
    WT QQLSREEKRRRRRATAKYRSAHATRERIRVEAFNLAFAELRKLLPTLPPDKKLSKIEILR
Nhlh2-m QQLSREEKRRAPARHGQVPIGPRH---PRAHPSGGFQPGLRRAPQTTTPDKKLSKIEILR
        **********     .:   .       *..  .     **:   *  ************
        helix
    WT LAICYISYLNHVLDV     135
Nhlh2-m LAICYISYLNHVLDV     132
        ***************
```

E

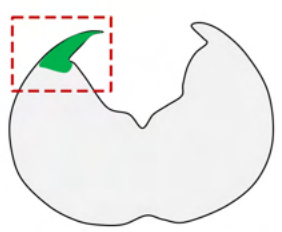

F

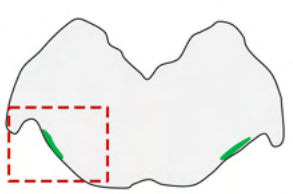

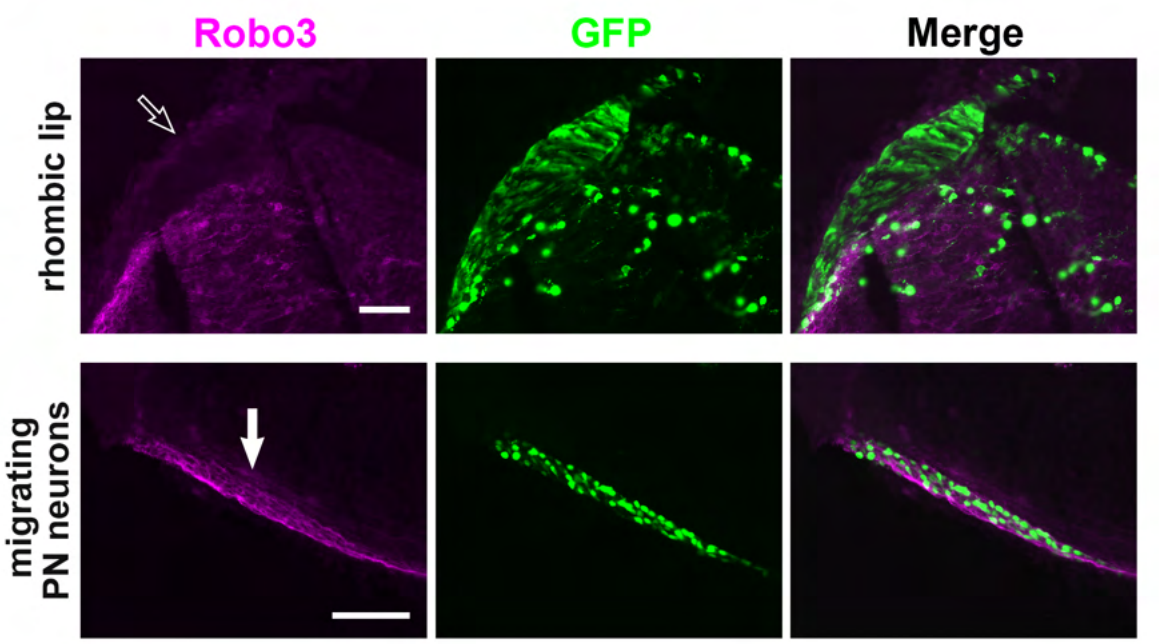

Supplemental Figure 8

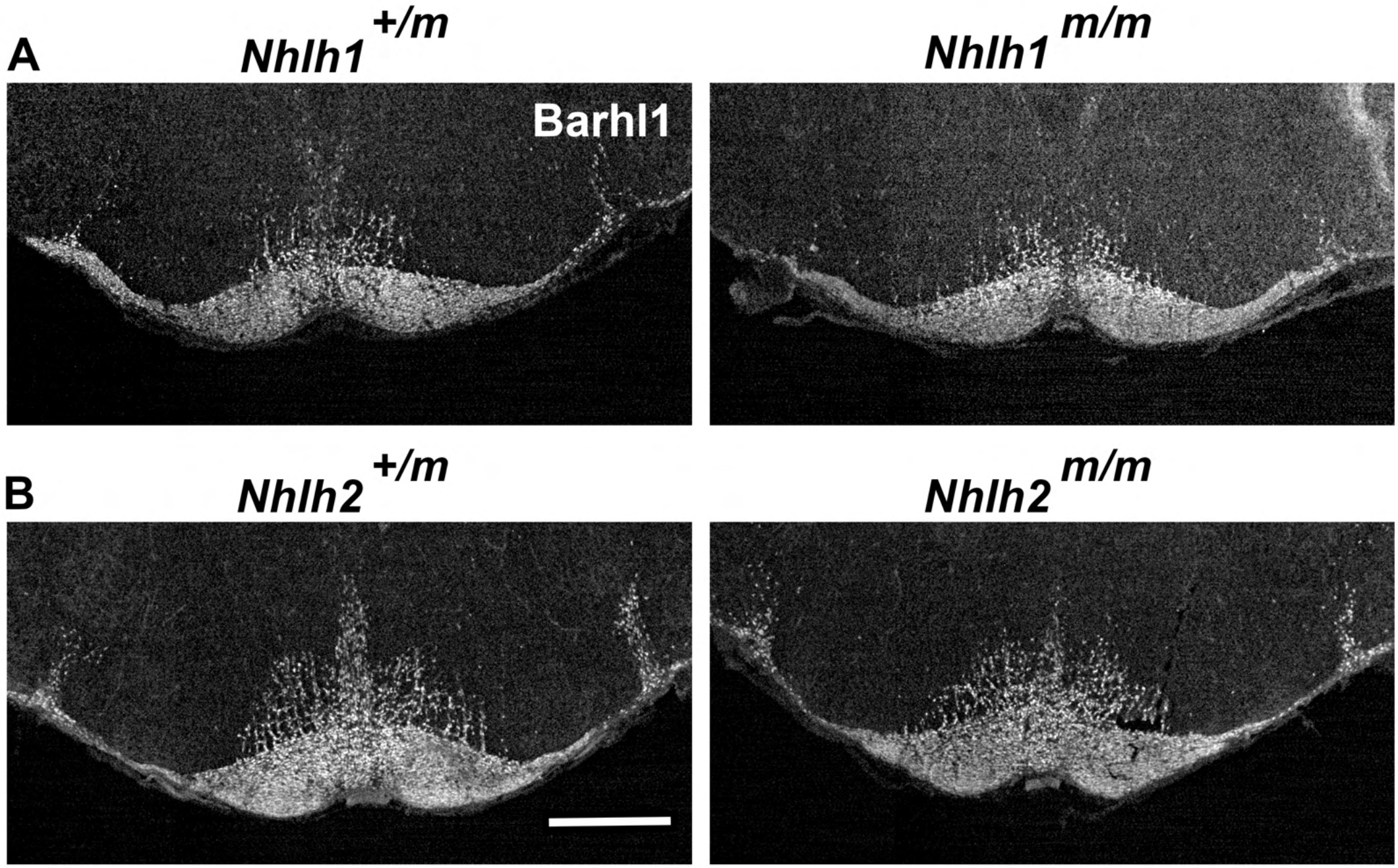

Supplemental Figure 9

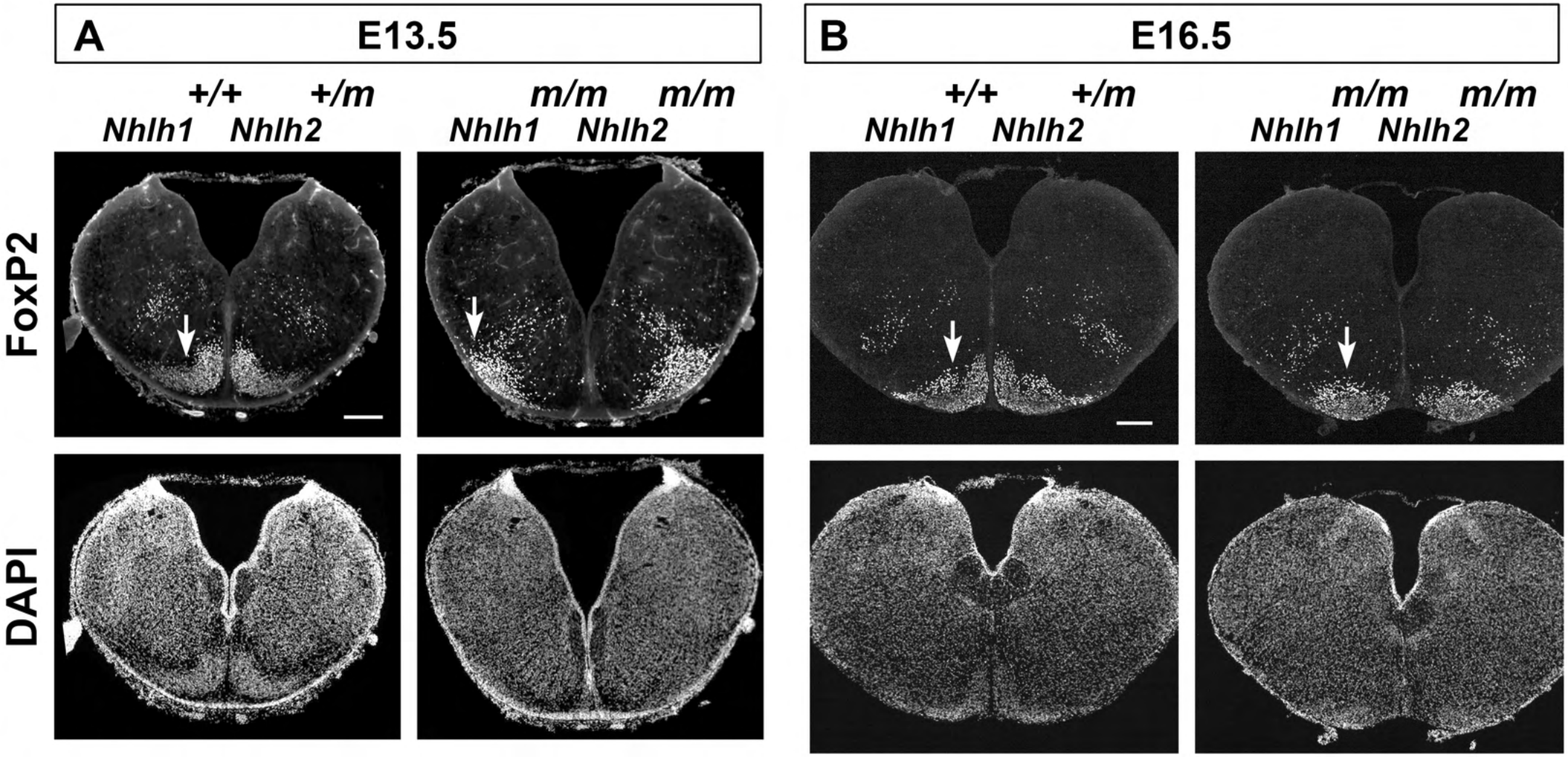

Supplemental Figure 10

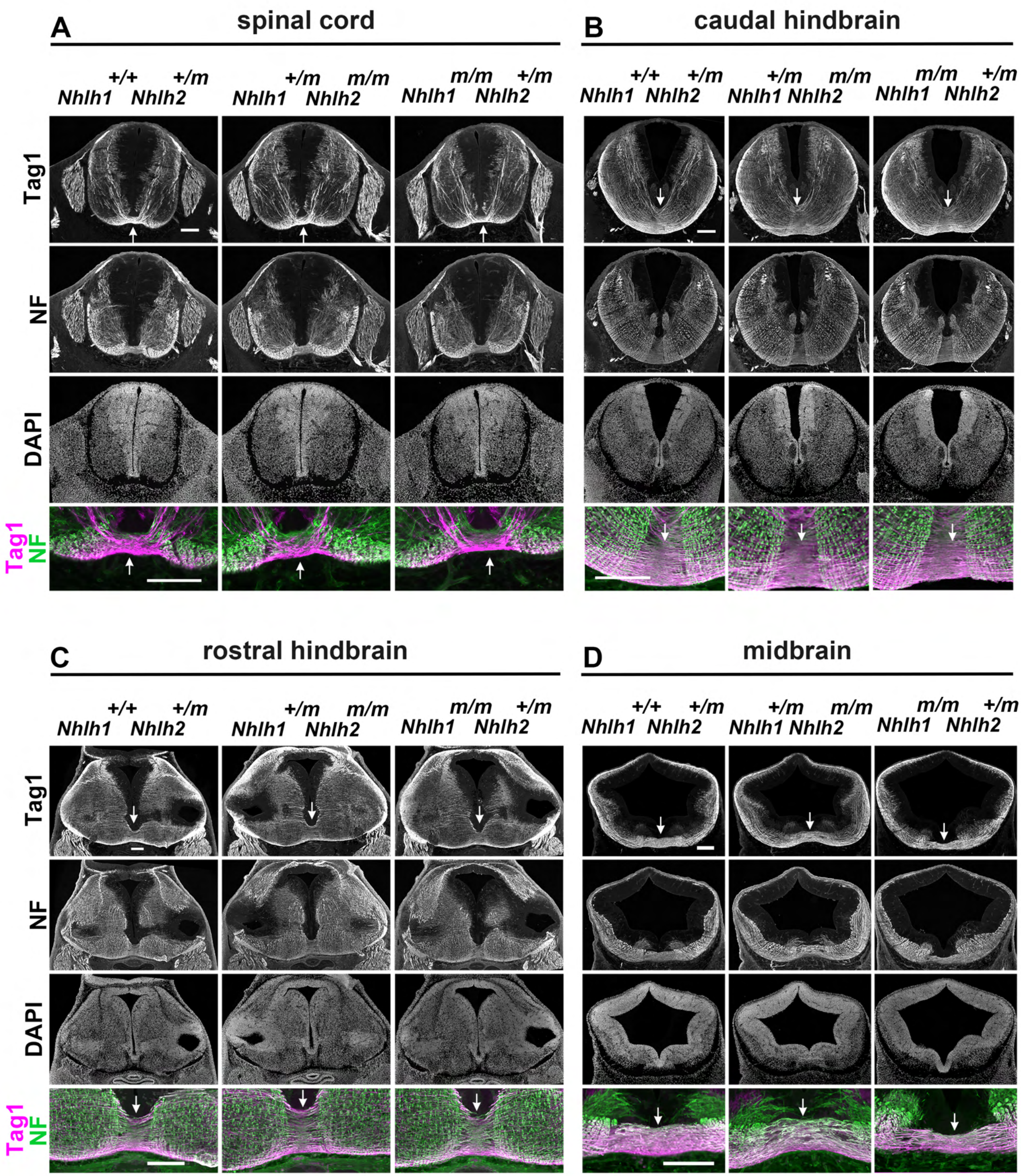

Supplemental Figure 11

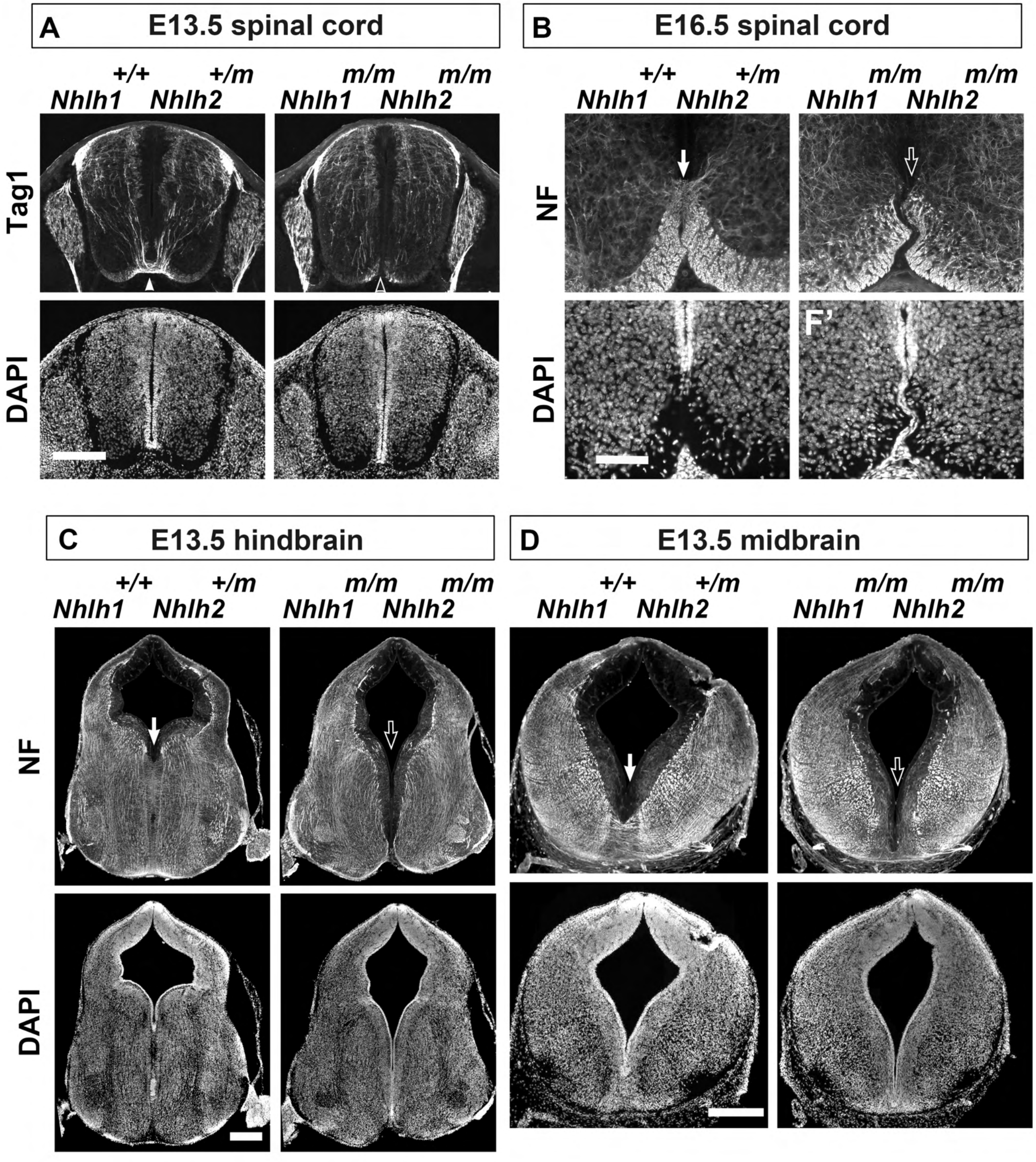

Supplemental Figure 12

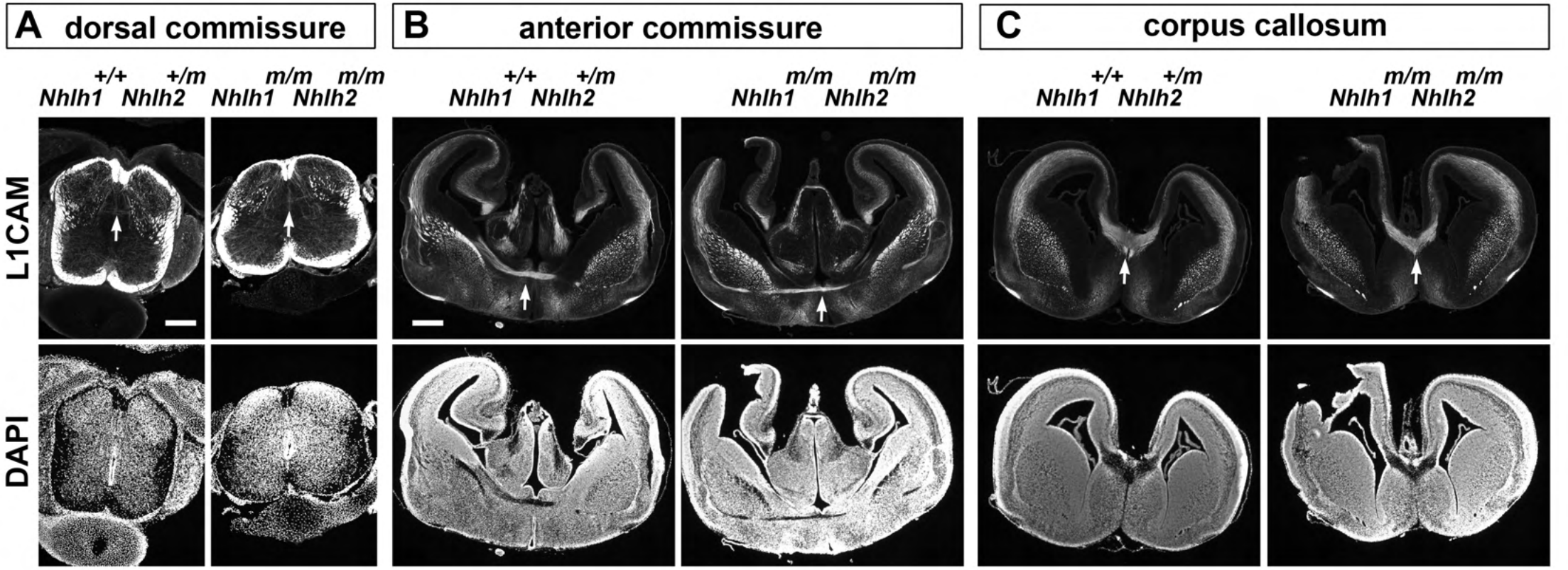

Supplemental Figure 13

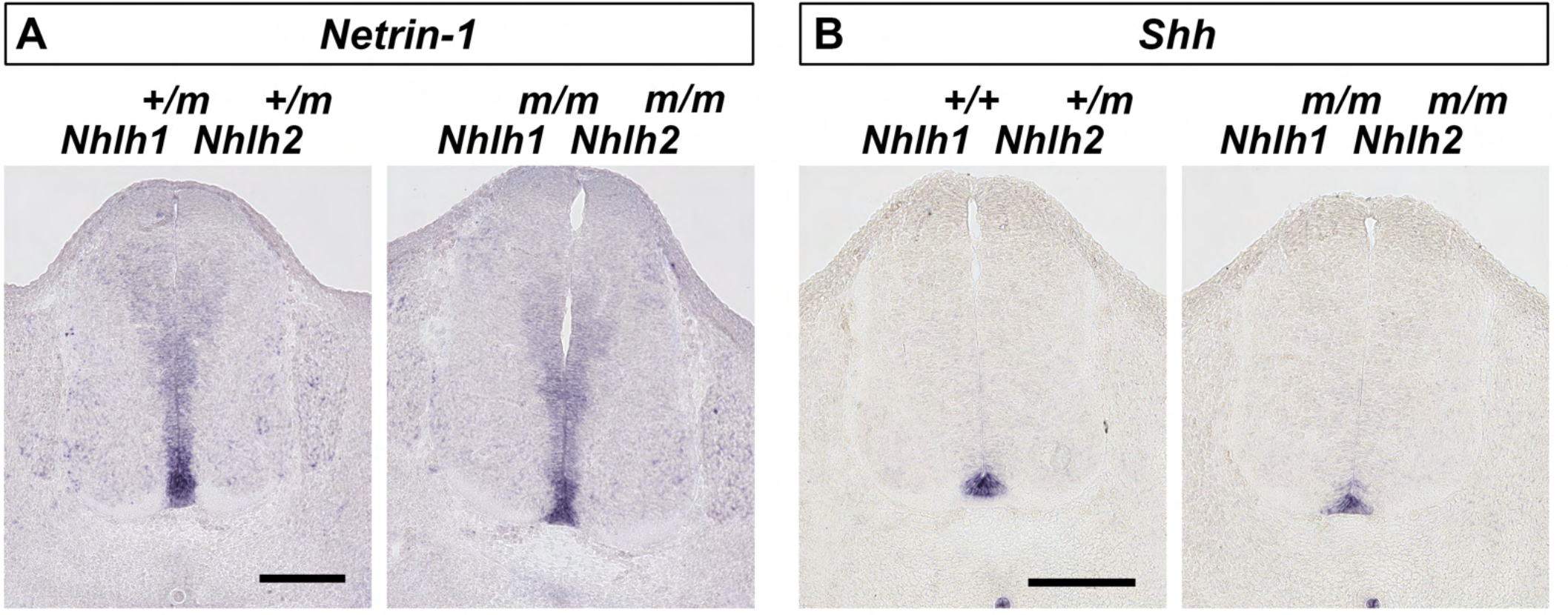

Supplemental Figure 14

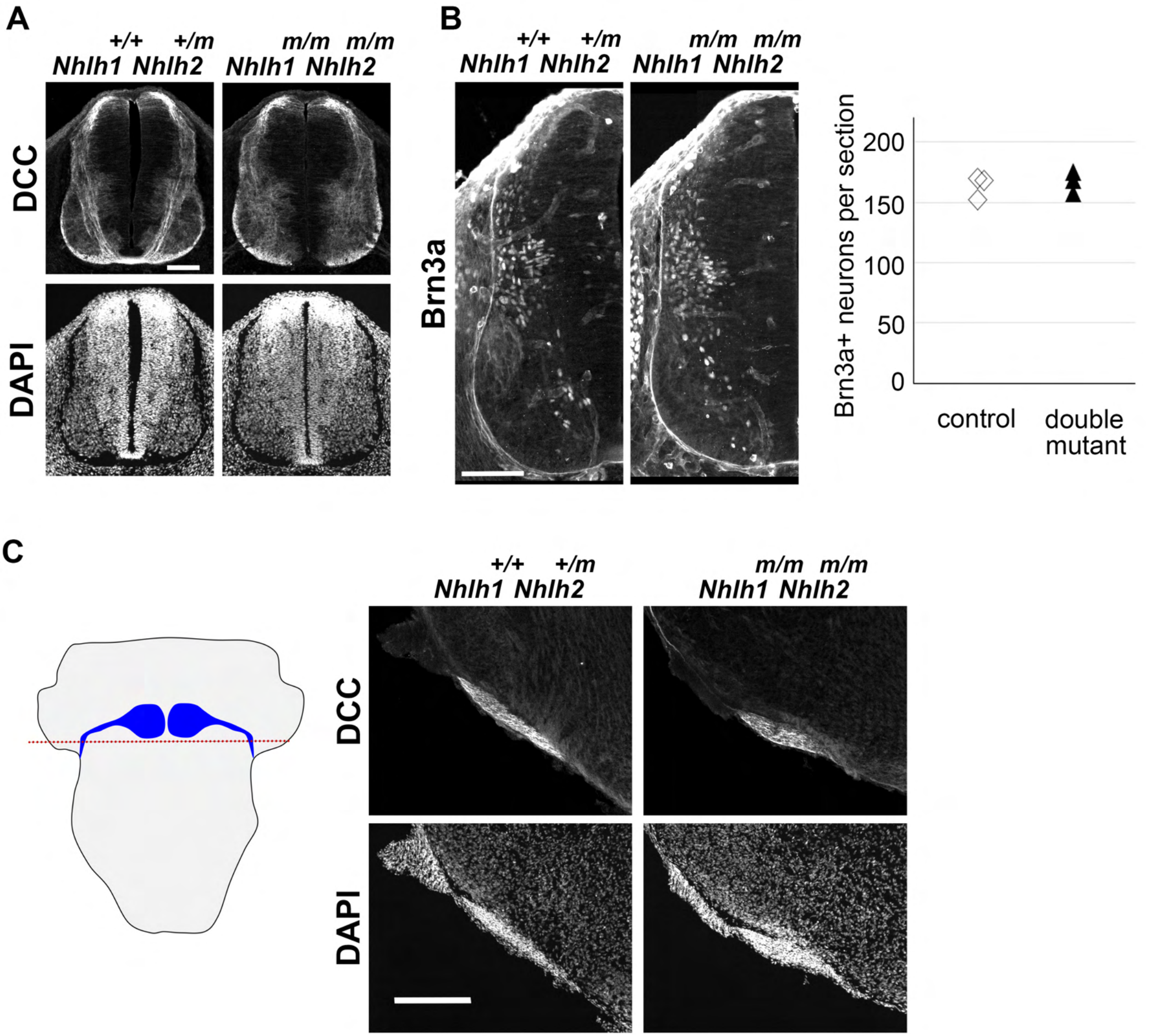

Supplemental Figure 15

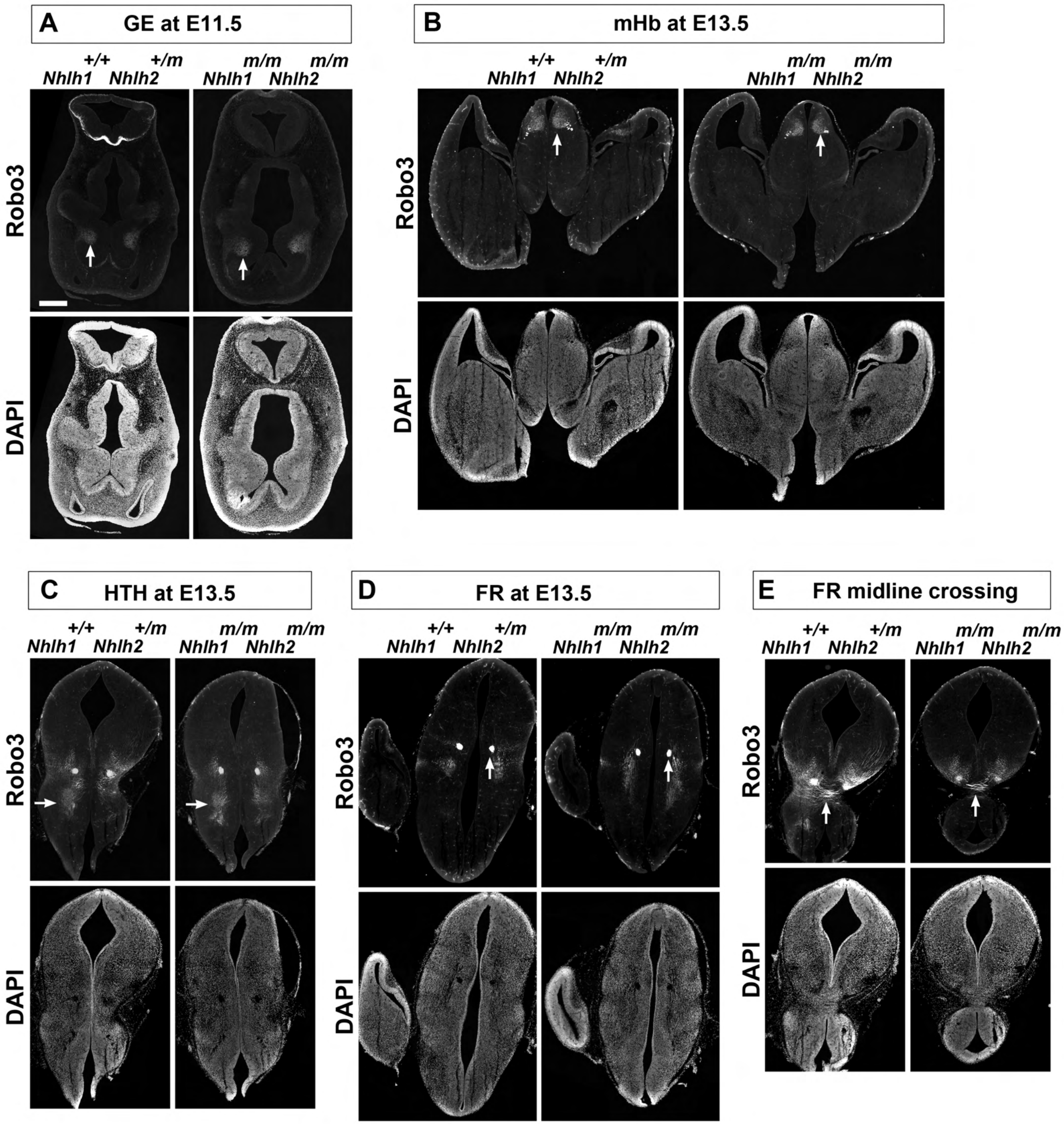

Supplementa Figure 16

A

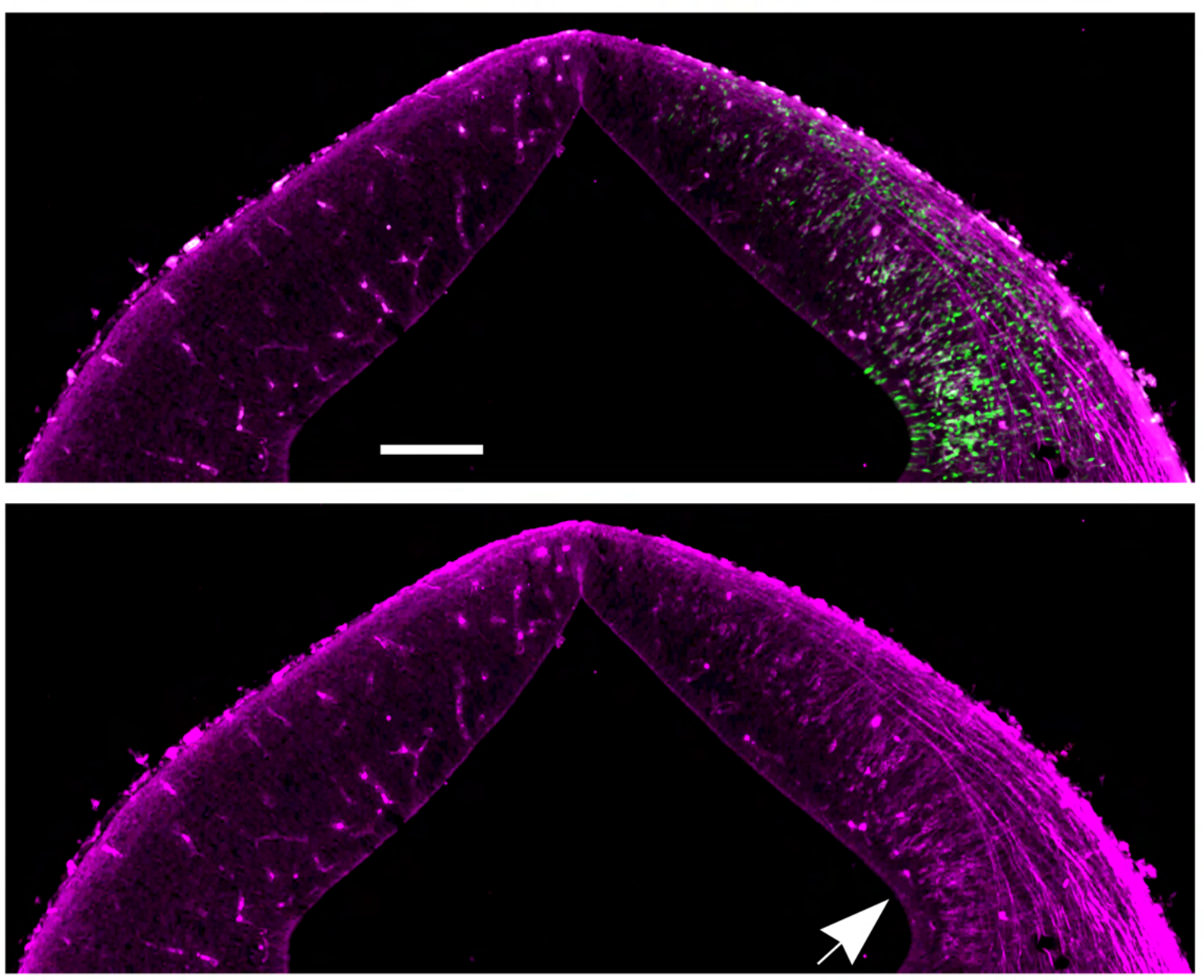

B

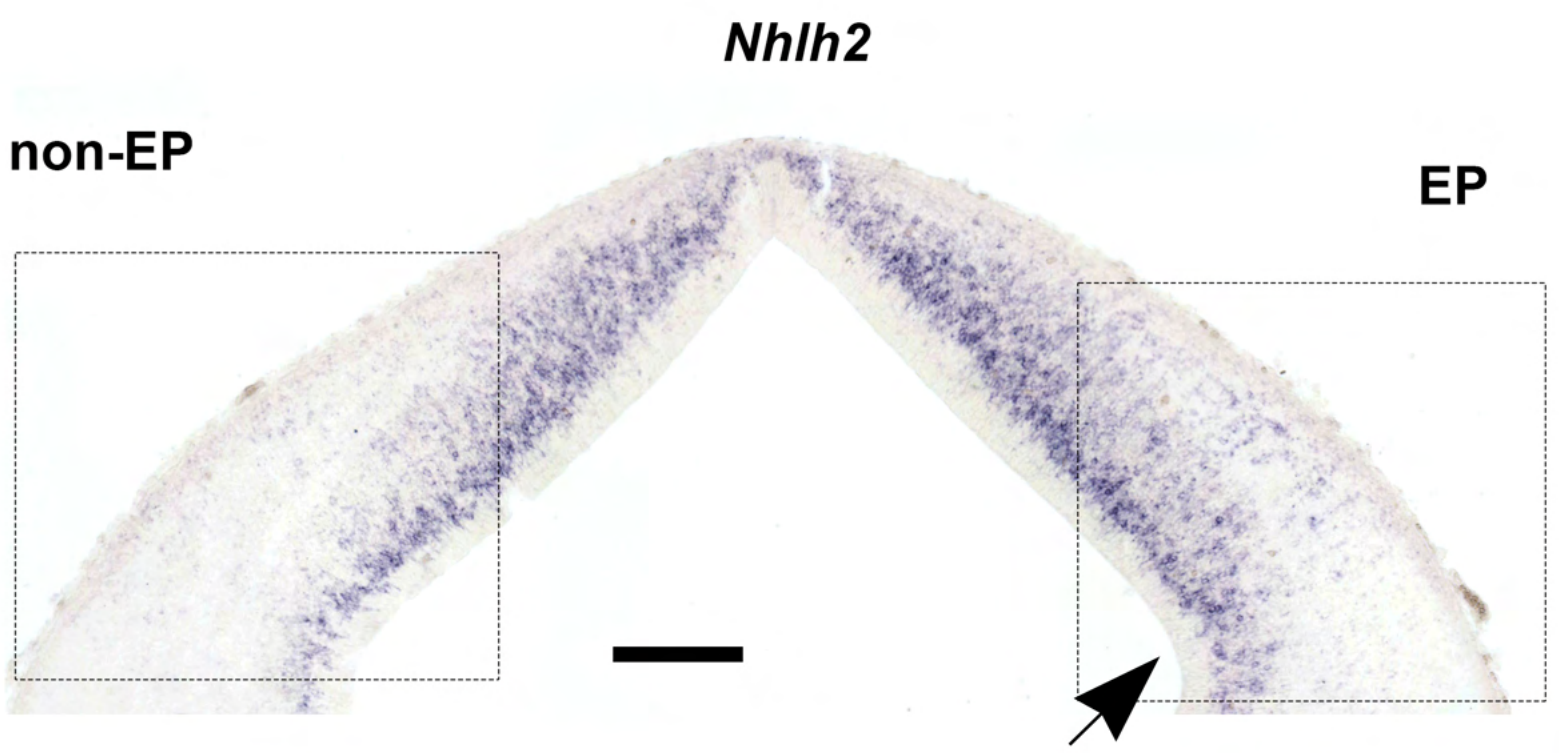
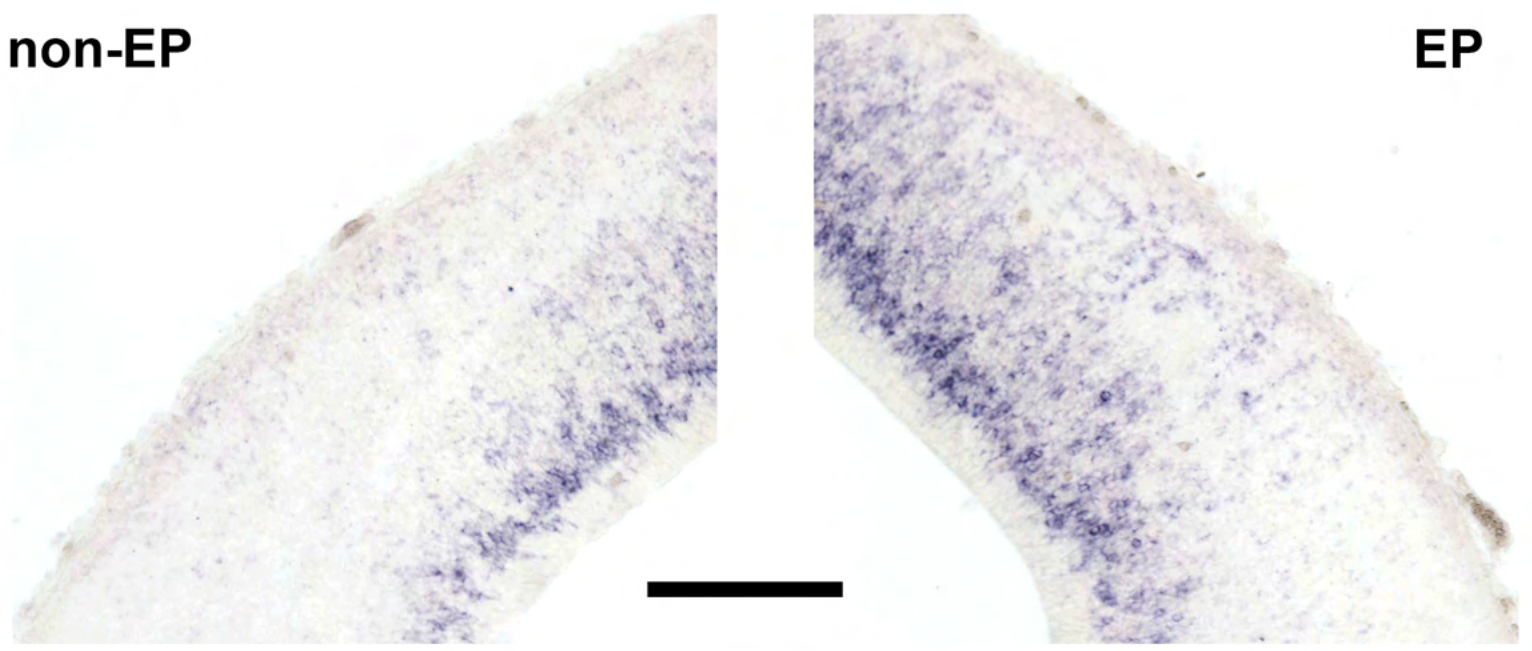
C